Published in final edited form as:
Earth Space Sci. 2020 July ; 7(7): . doi:10.1029/2020ea001098.

Characterization of Aerosol Hygroscopicity Over the Northeast Pacific Ocean: Impacts on Prediction of CCN and Stratocumulus Cloud Droplet Number Concentrations

B. C. Schulze[1], **S. M. Charan**[2], **C. M. Kenseth**[2], **W. Kong**[2], **K. H. Bates**[3], **W. Williams**[4], **A. R. Metcalf**[4], **H. H. Jonsson**[5], **R. Woods**[5], **A. Sorooshian**[6,7], **R. C. Flagan**[8,2], **J. H. Seinfeld**[8,2]

[1]Department of Environmental Science and Engineering, California Institute of Technology, Pasadena, CA, USA,

[2]Division of Chemistry and Chemical Engineering, California Institute of Technology, Pasadena, CA, USA,

[3]Center for the Environment, Harvard University, Cambridge, MA, USA,

[4]Department of Environmental Engineering and Earth Sciences, Clemson University, Anderson, SC, USA,

[5]Naval Postgraduate School, Monterey, CA, USA,

[6]Department of Chemical and Environmental Engineering, University of Arizona, Tucson, AZ, USA,

[7]Department of Hydrology and Atmospheric Sciences, University of Arizona, Tucson, AZ, USA,

[8]Division of Engineering and Applied Science, California Institute of Technology, Pasadena, CA, USA

Abstract

During the Marine Aerosol Cloud and Wildfire Study (MACAWS) in June and July of 2018, aerosol composition and cloud condensation nuclei (CCN) properties were measured over the N.E. Pacific to characterize the influence of aerosol hygroscopicity on predictions of ambient CCN and stratocumulus cloud droplet number concentrations (CDNC). Three vertical regions were characterized, corresponding to the marine boundary layer (MBL), an above-cloud organic aerosol layer (AC-OAL), and the free troposphere (FT) above the AC-OAL. The aerosol hygroscopicity parameter (κ) was calculated from CCN measurements (κ_{CCN}) and bulk aerosol mass spectrometer (AMS) measurements (κ_{AMS}). Within the MBL, measured hygroscopicities varied

Correspondence to: J. H. Seinfeld, seinfeld@caltech.edu.

Data Availability Statement
Airborne field data used in this work can be accessed on the Figshare database (Sorooshian et al., 2017: https://doi.org/10.6084/m9.figshare.5099983.v10).

Supporting Information:
Supporting Information S1

between values typical of both continental environments (~0.2) and remote marine locations (~0.7). For most flights, CCN closure was achieved within 20% in the MBL. For five of the seven flights, assuming a constant aerosol size distribution produced similar or better CCN closure than assuming a constant "marine" hygroscopicity ($\kappa = 0.72$). An aerosol-cloud parcel model was used to characterize the sensitivity of predicted stratocumulus CDNC to aerosol hygroscopicity, size distribution properties, and updraft velocity. Average CDNC sensitivity to accumulation mode aerosol hygroscopicity is 39% as large as the sensitivity to the geometric median diameter in this environment. Simulations suggest CDNC sensitivity to hygroscopicity is largest in marine stratocumulus with low updraft velocities (<0.2 m s^{-1}), where accumulation mode particles are most relevant to CDNC, and in marine stratocumulus or cumulus with large updraft velocities (>0.6 m s^{-1}), where hygroscopic properties of the Aitken mode dominate hygroscopicity sensitivity.

1. Introduction

Marine stratocumulus (MSc) clouds, commonly observed off the Western coasts of North America, South America, Africa, and Australia, cover nearly one fifth of the Earth's surface and exert a large impact on its radiative balance (Wood, 2012). These cloud decks are particularly relevant to global climate due to their high albedo contrast with the underlying ocean and relatively low altitude, resulting in stronger shortwave reflectance than longwave absorption (Brenguier et al., 2000; Randall et al., 1984; Wood, 2012). Previous estimates suggest that a ~12% increase in the albedo of these clouds would produce a negative radiative forcing equivalent in magnitude to that of doubling atmospheric CO_2 concentrations (Latham et al., 2008; Stevens & Brenguier, 2009). Remote sensing, parcel modeling, and large eddy simulation (LES) studies have all established that MSc exhibit substantial albedo susceptibility to variations in cloud droplet number concentrations (CDNC) (Berner et al., 2015; Chen et al., 2011; Oreopoulos & Platnick, 2008; Platnick & Twomey, 1994; Sanchez et al., 2016). Understanding the sensitivity of MSc CDNC to aerosols acting as cloud condensation nuclei (CCN) is therefore a critical aspect of reducing uncertainty in climate change predictions (Seinfeld et al., 2016).

The CDNC and albedo of MSc are substantially influenced by the abundance of below-cloud CCN. A recent satellite analysis suggested that variability in below-cloud CCN concentration may be responsible for ~45% of the variability in the radiative effect of marine boundary layer clouds (Rosenfeld et al., 2019). This influence results from the fact that increased CCN abundance enhances cloud reflectivity at constant liquid water path (Twomey, 1977) and has the potential to reduce MSc precipitation rates, increasing cloud lifetime (Ackerman et al., 1993; Albrecht, 1989; Goren & Rosenfeld, 2012; Rosenfeld, 2006). As a result, a major component of the uncertainty in the estimated indirect aerosol forcing has been attributed to the prediction of below-cloud CCN concentrations (Rosenfeld et al., 2014; Sotiropoulou et al., 2007). While the aerosol size distribution is generally thought to be the most important determinant of CCN activity (e.g., Dusek et al., 2006; Ervens et al., 2007; McFiggans et al., 2006; Reutter et al., 2009), particle composition has also been shown to exert a substantial influence (Jimenez et al., 2009; Liu & Wang, 2010; Mei et al., 2013; Quinn et al., 2008; Sanchez et al., 2016).

The propensity of a given aerosol particle to act as a CCN can be described using Köhler theory (Köhler, 1936; Seinfeld et al., 2016), provided sufficient information is known regarding particle size and solute properties (e.g., molecular weight, solubility, density, and activity). A novel framework, κ-Köhler theory, condenses these solute characteristics into a single parameter κ (the aerosol hygroscopicity) that can be easily incorporated into large-scale models (Petters & Kreidenweis, 2007). Substantial effort has, therefore, been devoted to quantifying κ values in a multitude of environments (Ervens et al., 2010; Gunthe et al., 2009; Pringle et al., 2010; Rose et al., 2010; Thalman et al., 2017). While κ values characteristic of inorganic aerosol components are relatively well-established, atmospheric organic aerosol is composed of numerous, highly diverse organic compounds, complicating representation of organic hygroscopicity using a single parameter (Kanakidou et al., 2005). Experimental studies have characterized κ values of secondary organic aerosol (SOA) (e.g., Asa-Awuku et al., 2010; Duplissy et al., 2008, 2011; Frosch et al., 2013; Lambe et al., 2011; Massoli et al., 2010; Zhao et al., 2015), and field studies have characterized the typical range of organic κ values (κ_{org}) observed in the atmosphere (Chang et al., 2010; Gunthe et al., 2009; Levin et al., 2014; Mei et al., 2013; Thalman et al., 2017; Wang et al., 2008). Generally, ambient κ_{org} values are found to be 0.1–0.2 for aged aerosol and primary marine organics and ~0 for freshly emitted combustion aerosol (e.g., soot) (Kreidenweis & Asa-Awuku, 2014). A linear relationship has been noted between observed κ_{org} values and organic aerosol oxygen-to-carbon (O:C) ratios in both the laboratory and the field (Chang et al., 2010; Lambe et al., 2011; Mei et al., 2013; Wang et al., 2019).

Ambient particle hygroscopicity data have been combined with aerosol size distribution measurements in CCN closure studies to assess the extent to which Köhler theory can be used to predict ambient CCN concentrations (e.g., Almeida et al., 2014; Asa-Awuku et al., 2011; Cubison et al., 2008; Medina et al., 2007; McFiggans et al., 2006; Moore et al., 2012; Ren et al., 2018; VanReken et al., 2003). Analyzing the accuracy of predicted CCN concentrations can provide insight into the influence of specific aerosol characteristics on CCN activity (Bougiatioti et al., 2011; Cubison et al., 2008; Medina et al., 2007; VanReken et al., 2003; Wang et al., 2010). For instance, size-resolved compositional (i.e., hygroscopicity) data are often required to accurately reproduce observed CCN concentrations in locations dominated by organic aerosol (Bhattu & Tripathi, 2015; Medina et al., 2007; Ren et al., 2018), while aerosol mixing state has been shown to strongly impact total CCN concentrations in urban environments (Cubison et al., 2008; Ervens et al., 2010; Quinn et al., 2008). By analyzing data from five ambient measurement campaigns, Ervens et al. (2010) found that for aerosol measured farther than a few tens of kilometers from the emission source, CCN activity could be predicted within a factor of two independent of either aerosol mixing state (i.e., internal or external) or organic solubility (i.e., insoluble or slightly soluble). Wang et al. (2010) further demonstrated that CCN concentrations can often be reproduced within 20% assuming internal mixing of aerosol components if the overall κ of the aerosol population is >0.1. The direct impact of variability in aerosol hygroscopicity on CCN concentrations is often assessed by assuming an invariant chemical composition, represented as a fixed κ, in CCN closure analyses. Field campaigns in continental environments ranging from polluted megacities to the pristine tropical rainforest have shown that CCN concentrations could be reproduced within 20% and 50%, respectively, assuming a

constant $\kappa = 0.3$ (Gunthe et al., 2009; Rose et al., 2010), a value representative of average continental conditions (Andreae & Rosenfeld, 2008; Pringle et al., 2010). However, in coastal regions, MBL aerosol can result from a mixture of distinct marine and continental emissions (e.g., Coggon et al., 2014; Mardi et al., 2018; Modini et al., 2015; Sorooshian et al., 2009), which complicates aerosol representation using regional or global models. CCN closure analysis can provide insight into the uncertainties in CCN concentrations that may result from inaccurate model representation of aerosol composition in these environments.

Due to the importance of the persistent stratocumulus cloud decks over the N.E. Pacific to global climate, aerosol characteristics in this region have received considerable attention. However, the diverse range of particle sources, including shipping exhaust (Coggon et al., 2012; Murphy et al., 2009; Prabhakar et al., 2014; Wonaschütz et al., 2013), primary and secondary natural marine emissions (Modini et al., 2015; Prabhakar et al., 2014; Sorooshian et al., 2009), anthropogenic and biogenic continental emissions (Coggon et al., 2014; Hegg et al., 2010; Moore et al., 2012), wildfire plumes (Brioude et al., 2009; Mardi et al., 2018), and aged aerosol from the Asian continent (Roberts et al., 2006, 2010), combined with strong temporal and spatial variability due to variable meteorological conditions, has hindered determination of general characteristics of the marine atmosphere in this location. This complexity is reflected in the diversity of hygroscopicity measurements previously reported in the marine boundary layer (MBL) and free troposphere (FT). For instance, average κ values reported from MBL measurements have varied from ~0.2–0.3 (Moore et al., 2012; Roberts et al., 2010) to ~0.5–0.7 (Royalty et al., 2017; Yakobi-Hancock et al., 2014). Measurements in the FT, while sparse, have been even more variable (κ ~0.05–1.0) (Roberts et al., 2006, 2010). While these measurements could largely be reconciled assuming various mixtures of continental (0.27 ± 0.2) and marine (0.72 ± 0.2) aerosol, determining the major emissions sources and meteorological patterns dictating these changes is important for improving model representation of the region (Pringle et al., 2010). CCN-based measurements of aerosol hygroscopicity and the resulting information about small particle composition can be especially useful in this regard, as knowledge of small particle composition can provide substantial insight into particle sources.

While hygroscopicity and mixing state characterization are important components of understanding the CCN activity of ambient aerosol, the dynamic processes controlling supersaturation, droplet nucleation, and droplet growth within clouds lead to nonlinear relationships between aerosol properties and CDNC. As a result, aerosol-cloud parcel modeling is instrumental to fully understand the role of aerosol hygroscopicity and mixing state on CDNC. Reutter et al. (2009) used such a model to distinguish three regimes of aerosol activation, defined as the aerosol-limited, updraft-limited, and transitional regimes, based on the ratio of updraft velocity to aerosol number concentration at the cloud base. The dependence of CDNC on aerosol hygroscopicity, while limited relative to other parameters such as particle number concentration and updraft velocity, was found to vary substantially between regimes. Additional modeling revealed that CDNC sensitivity to aerosol hygroscopicity is highly dependent on the below-cloud aerosol size distribution, with sensitivity increasing substantially with smaller median radii (Ward et al., 2010). Sanchez et al. (2016) concluded that modeled stratocumulus albedo is insensitive to the assumed

hygroscopicity of the organic aerosol fraction; however, the sensitivity of CDNC to bulk hygroscopicity has yet to be fully evaluated in this environment.

The present study uses measurements of aerosol composition and CCN activity collected during the Marine Aerosol Cloud and Wildfire Study (MACAWS), combined with an aerosol-cloud parcel model, to gain insight into near-coastal aerosol hygroscopicity and its influence on prediction of CCN and MSc CDNC. Hygroscopicity measurements are combined with airmass backward trajectories and meteorological parameters to attribute observed particle characteristics to distinct sources when possible. CCN closure analyses are performed to investigate the impact of compositional and mixing state assumptions on CCN predictions. Finally, aerosol-cloud parcel model simulations constrained with MSc microphysical measurements are used to directly investigate the sensitivity of stratocumulus CDNC to aerosol hygroscopicity, mixing state, and size distribution properties.

2. Methodology

2.1. MACAWS Field Mission

The 2018 Marine Aerosol Cloud and Wildfire Study (MACAWS) consisted of 16 research flights operated out of the Center for Interdisciplinary Remotely-Piloted Aircraft Studies (CIRPAS) in Marina, California, during June and July. Measurements were performed on-board the CIRPAS Navy Twin Otter aircraft (Coggon et al., 2012, 2014; Russell et al., 2013; Sorooshian et al., 2019; Wang et al., 2016). The scientific objectives of individual flights included characterization of marine aerosols and clouds, sampling of shipping vessel exhaust plumes, and investigation of nearby wildfire emissions. The present study focuses on seven research flights primarily aimed at characterization of the relationship between marine aerosol and the overlying stratocumulus cloud deck. Paths of these seven flights are depicted in Figure 1. Flight strategies typically involved a series of level legs at varying altitudes within the MBL and overlying FT. Slant or spiral soundings were generally performed before and after a series of level legs.

2.2. Twin Otter Instrumentation

The navigational and meteorological instrumentation utilized by the Twin Otter aircraft is described in detail by Sorooshian et al. (2018). Ambient aerosol was sampled using a forward-facing sub-isokinetic inlet (Hegg et al., 2005). Aerosol and cloud droplet number concentrations were characterized using a variety of instruments, including multiple condensation particle counters (CPC, TSI 3010, D_p > 10 nm; ultrafine CPC, TSI UFCPC, D_p > 3 nm), a passive cavity aerosol spectrometer probe (PCASP, D_p ~0.11–3.4 μm), and forward scattering spectrometer probe (FSSP, Particle Measuring Systems [PMS], D_p ~1.6–45 μm). Cloud liquid water content was measured using a PVM-100A probe (Gerber et al., 1994), and a threshold value of 0.02 g m^{-3} was used to distinguish in-cloud sampling (Dadashazar et al., 2018; MacDonald et al., 2018).

Cloud condensation nuclei (CCN) number concentrations were measured at four supersaturations (SS) (0.1%, 0.3%, 0.43%, and 0.57%) using a Droplet Measurement Technologies (DMT) dual-column streamwise thermal-gradient cloud condensation nuclei

counter (CCNC) (Lance et al., 2006; Roberts & Nenes, 2005). The CCNC operates by applying a linear temperature gradient to a cylindrical sampling tube with continuously wetted walls. As the thermal diffusivity of water vapor exceeds the diffusivity of air, supersaturated conditions are produced along the sampling column centerline. For this study, activated droplets grown to sizes larger than 0.75-μm diameter were counted and sized by an optical particle counter. The sheath and sample flows of each column were maintained at 0.45 and 0.05 L min^{-1}, respectively. Instrument pressure was maintained at 750 mb using a flow orifice and active pressure control system at the instrument inlet. Each column of the CCNC was calibrated using ammonium sulfate particles following standard methods as described in Rose et al. (2008). Calibrations were performed before and after the campaign, and observed deviations in applied SS for a given temperature gradient imply uncertainties of ~6%, similar to the 5% value typical of field campaigns, as reported by Rose et al. (2008).

Aerosol size distributions and number concentrations for D_p between ~15 and 800 nm were measured with a custom-built scanning mobility particle sizer (SMPS) consisting of a differential mobility analyzer (DMA, TSI 3081) coupled to a condensation particle counter (TSI 3010). The DMA is operated in a closed-system configuration with a recirculating sheath and excess flow of 2.67 L min^{-1} and an aerosol flow of 0.515 L min^{-1}. The column voltage was scanned from 15 to 9,850 V over a ~2-min interval.

Aerosol chemical composition was measured using a high-resolution time-of-flight aerosol mass spectrometer (HR-ToF-AMS, Aerodyne Research Inc., hereafter referred to AMS) (DeCarlo et al., 2006). Incoming air enters the AMS through a 100-μm critical orifice, after which an aerodynamic lens produces a particle beam that is accelerated under high vacuum. The particle beam is flash-vaporized on a resistively heated surface (600°C), and the resulting gases are ionized by electron impaction (70 eV). Individual ion identity is determined using a high-resolution time-of-flight mass spectrometer. Due to the limited amount of aerosol mass present over the MBL, data were collected in high-sensitivity V-mode. The ionization efficiency (IE) of the AMS was calibrated using dry, 350-nm ammonium nitrate particles before each flight. Data were averaged over 1-min intervals, and all data were analyzed using standard AMS software (SQUIRREL v1.57 and PIKA v1.16l) within Igor Pro 6.37. The collection efficiency (CE) was determined using the composition-dependent calculator within the SQUIRREL and PIKA software packages (Middlebrook et al., 2012). Elemental H:C and O:C ratios were calculated using the “Improved-Ambient” elemental analysis method for AMS mass spectra (Canagaratna et al., 2015). Positive matrix factorization (PMF) analysis (Paatero & Tapper, 1994) was performed on the high-resolution AMS mass spectra in order to distinguish major classes and transformation processes of measured OA. Three factors were extracted, two of which factors correspond to OA subtypes characteristic of the MBL and above-cloud organic aerosol layer (AC-OAL), respectively, and resemble low-volatility oxygenated organic aerosol (LV-OOA). The third factor, which was rarely observed, is likely a result of primary anthropogenic emissions and resembles hydrocarbon-like organic aerosol (HOA). Further discussion of PMF data preparation and factor interpretation is included in the supporting information.

2.3. Determination of Aerosol Hygroscopicity

Aerosol hygroscopicity was calculated using two distinct methods based on measurements with the CCNC and AMS, respectively. Assuming a particle population is internally mixed, the critical activation diameter ($D_{p,c}$) (the diameter at which all larger particles will activate into cloud droplets) produced by a given SS can be determined by integrating the particle size distribution until the total CN concentration is equivalent to the measured CCN concentration:

$$N_{CCN} = \int_{D_{p,c}}^{\infty} n_{CN} dD_p \tag{1}$$

Knowledge of the critical diameter can then be used to calculate a single parameter representation of aerosol hygroscopicity from Köhler theory (Petters & Kreidenweis, 2007):

$$s = \frac{D_{wet}^3 - D_{p,c}^3}{D_{wet}^3 - D_{p,c}^3(1-\kappa_{CCN})} \exp\left(\frac{4\sigma M_w}{RT\rho_w D_{wet}}\right) \tag{2}$$

where s is the equilibrium supersaturation, $D_{p,c}$ is the critical activation diameter, D_{wet} is the droplet diameter, R is the universal gas constant, T is the absolute temperature, ρ_w is the molar density of water, M_w is the molecular weight of water, and σ is the surface tension of the droplet at the point of activation. Following Rose et al. (2010), κ was determined by applying the observed activation diameter and varying both D_{wet} and κ until s is equivalent to the applied supersaturation of the CCNC and the maximum of a Köhler curve of CCN activation. The droplet surface tension is assumed equal to that of water for comparison with other studies (Collins et al., 2013; Petters & Kreidenweis, 2007; Roberts et al., 2010; Yakobi-Hancock et al., 2014). Hygroscopicity values calculated using this method are referred to as "CCN-derived." Since the likelihood of particle activation at a given SS tends to be a stronger function of size than composition (Dusek et al., 2006), κ_{CCN} values correspond to particles with diameters near the calculated critical diameter.

A Monte Carlo approach was used to estimate the uncertainty in CCN-derived kappa values (Wang et al., 2019). A detailed description is provided in the supporting information. For a given measurement of the aerosol size distribution and CCN number concentration, the distribution of possible κ_{CCN} values calculated by varying these input parameters (i.e., CCN number concentration and size distribution) within their respective uncertainties is lognormally distributed. As a result, uncertainties attributed to κCCN are not symmetric about the geometric mean values. In general, we estimate 1σ uncertainties of +55%/−40% for κ_{CCN} calculated at SS = 0.3%, ~+75%/−45% at SS = 0.43%, and +100%/−50% to values calculated at SS = 0.57%. Due to the low CCN number concentrations observed at SS = 0.1% (<100 cm^{-3}) and possibility of counting unactivated particles (expected to only be a few per cm^{-3}), κ_{CCN} at SS = 0.1% are not reported, as small absolute deviations in particle number concentration measured by the CCNC and DMA due to differential inlet losses could strongly influence the resulting κ_{CCN} estimates.

Hygroscopicity estimates can also be made using component volume fractions measured by the HR-ToF-AMS using the following equation (Petters & Kreidenweis, 2007):

$$\kappa_{AMS} = \sum_{i}^{N} \epsilon_i \kappa_i \quad (3)$$

where ϵ_i and κ_i represent the volume fraction and hygroscopicity of the ith NR-PM_1 component, respectively. While this calculation cannot capture the contribution of refractory components (sea salt, mineral dust, etc.), further analysis suggests their contribution is minor, as discussed in the supporting information. Organic aerosol density was assumed to be 1.4 g cm^{-3} for volume fraction calculations given the remote nature of the environments sampled and the oxidized character of the measured organic aerosol (e.g., O:C ratios of MBL and AC-OAL PMF factors were 0.91 and 0.76, respectively) (Hallquist et al., 2009; Roberts et al., 2010). The hygroscopicity of individual inorganic components is calculated using

$$\kappa_i = \left(\frac{M_w}{\rho_w}\right)\left(\frac{\rho_i}{M_i}\right)\upsilon_i \quad (4)$$

where M_w and ρ_w are the molar mass and density of water, respectively, and M_i, ρ_i, and υ_i are the molar mass, density, and van't Hoff factor of the inorganic component. Inorganic aerosol was dominated by sulfate and ammonium. The relative abundances of ammonium sulfate, ammonium bisulfate, and sulfuric acid were calculated using the molar ratio of ammonium to sulfate (Asa-Awuku et al., 2011; Nenes et al., 1998). Ammonium sulfate and bisulfate were assigned van't Hoff factors of 2.5, while sulfuric acid was assigned $\kappa = 0.9$ to align with previous measurements (Petters & Kreidenweis, 2007). Modifying the van't Hoff factors of ammonium sulfate and ammonium bisulfate and assumed κ of sulfuric acid within reasonable limits had a negligible influence on the presented results. Chloride measured by the AMS was assumed to represent sodium chloride and was assigned a hygroscopicity of 1.28 (Petters & Kreidenweis, 2007). AMS-measured nitrate aerosol was assumed to be ammonium nitrate with a hygroscopicity of 0.67 (Petters & Kreidenweis, 2007). The hygroscopicity of the organic component (κ_{org}) was assumed to be either 0 (non-hygroscopic), 0.1 (slightly-hygroscopic), or a function OA composition using a parameterization based on bulk O:C ratios developed in the literature (Lambe et al., 2011). Comparisons of κ_{CCN} and κ_{AMS} values, analysis of PMF factor composition, and evaluation of CCN-closure calculations are used to evaluate these different κ_{org} estimates.

An uncertainty analysis similar to that described for κ_{CCN} values was performed for κ_{AMS} values and is described in detail in the supporting information. For median conditions in the MBL and FT, the relative uncertainty in κ_{AMS} is estimated to be ~10–20%, due primarily to uncertainty in the estimated hygroscopicity of the organic component (κ_{org}). In the AC-OAL, the dominant contribution of organic aerosol increases the relative uncertainty to ~50%; however, due to the low absolute κ_{AMS} values observed in the AC-AMS OAL, the absolute uncertainty is only ~0.1 or less.

2.4. Aerosol-Cloud Parcel Model

The aerosol-cloud parcel model used in this study employs a user-specified updraft velocity to induce adiabatic cooling of an air parcel, leading to water vapor supersaturation. The predicted parcel supersaturation at each time step is determined by the relative rates of production through adiabatic cooling and loss through condensation of water vapor onto activated cloud droplets (Pruppacher & Klett, 1997; Seinfeld et al., 2016). In the present study, meteorological parameters such as ambient pressure, temperature, and lapse rate are obtained from MACAWS aircraft measurements and are specified before model execution. The below-cloud dry size distribution is assumed to contain Aitken and accumulation modes, the characteristics of which (i.e., number concentration, geometric mean diameter, hygroscopicity) are set by the user. Particles within each mode can be specified as either internally or externally mixed. Each compositional class, 1 per size mode if internally mixed or 2 per size mode if externally mixed, contains 300 lognormally spaced bins ranging from 1 nm to 3 μm. Droplet activation is assumed to occur when the ambient supersaturation of the parcel exceeds the critical supersaturation of the particles in a given size bin, as determined from κ-Kohler theory (Petters & Kreidenweis, 2007). Following activation, the growth of individual cloud droplet bins due to water vapor diffusion is explicitly represented. Additional physical processes such as droplet coagulation, coalescence, and deposition are not included, as previous parcel model studies have demonstrated that these processes have little influence on model predictions for typical marine stratocumulus conditions (Sanchez et al., 2016). Model execution proceeds until a user-specified liquid water content (0.4 g m^{-3} in this study) has been reached. Activated particle size bins larger than 1 μm are considered cloud droplets; however, using an alternative size threshold of 2 μm or 0.75 μm has a negligible influence on the results.

2.5. Air Mass Backward Trajectories

Air mass backward trajectories (120 hr) were calculated in the MBL for each flight using the NOAA HYSPLIT v4.2 model with the global data assimilation system (GDAS) 1° × 1° meteorological data set (Draxler & Hess, 1997, 1998; Stein et al., 2015). The higher spatial resolution EDAS 40 km × 40 km meteorological data set was not used due to its limited spatial range over the Pacific Ocean. The ending altitude of each trajectory was the approximate midpoint of the MBL during each flight.

3. Results and Discussion

3.1. Aerosol Characteristics Over the N.E. Pacific

Results from the seven flights analyzed in this study are summarized in Figure 2 and Tables 1–3. In the subsequent analyses, “all flights” refers to these seven. Typical flight patterns included sampling within the MBL, FT, and, when present, the above-cloud organic aerosol layer (AC-OAL). The AC-OAL is operationally defined as the narrow altitude band (generally <200 m) directly above the marine stratocumulus cloud decks where OA mass loadings were relatively large (>1.5 μg m^{-3}) and a distinct AC-OAL PMF factor contributed >80% of total OA mass (Figure S6). This region occupies a similar location as the commonly referenced entrainment interface layer (EIL) above cloud decks (Dadashazar et al., 2018; Wood, 2012), but is defined by the aerosol characteristics described above rather

than by turbulence and buoyancy characteristics, as is common for the EIL (Carman et al., 2012). Median aerosol properties are reported in Tables 1–3 for each of these three regions, while Figure 2 displays vertical profiles of aerosol and meteorological properties.

Distinct differences in particle properties were observed within each vertical region. Median aerosol number concentrations observed in the MBL (754 cm^{-3}) exceeded those in the FT (333 cm^{-3}), as expected. Observed particle concentrations were maximized within the AC-OAL (1,662 cm^{-3}), where intense actinic fluxes and elevated concentrations of the hydroxyl radical may drive new particle formation (Dadashazar et al., 2018; Mauldin et al., 1999). For all measured SS > 0.1%, observed CCN concentrations were also largest within the AC-OAL, rather than the MBL or FT, underscoring the importance of understanding the hygroscopicity of above-cloud CCN-active particles (Coggon et al., 2014; Sorooshian, Lu, et al., 2007; Sorooshian et al., 2007; Wang et al., 2008).

Observed aerosol composition in the MBL was relatively evenly divided between organic aerosol (OA) (43%) and sulfate (SO_4) (48%), with a minor contribution from ammonium (NH_4) (~10%) and negligible nitrate (NO_3) (≤1%). Prabhakar et al. (2014) have demonstrated that nitrate is preferentially distributed in super-micron particles in this marine environment, in agreement with the minor contribution observed with the AMS in this study. Using the “clean” versus “perturbed” threshold introduced by Coggon et al. (2012) for this region (where “clean” is defined by aerosol mass concentrations <1 μg m^{-3}), average MBL conditions were “perturbed” by shipping vessel emissions or other anthropogenic sources such as continental outflow. A distinct, highly oxidized MBL PMF factor was extracted from the data set (Figure S6). The oxidized nature of the MBL factor (O:C = 0.91) precludes the use of marker ions to distinguish individual sources; however, potential sources include shipping and biogenic emissions, as well as oxidized continental outflow aerosol (Coggon et al., 2012; Hegg et al., 2010; Sorooshian et al., 2009). In the AC-OAL, observed aerosol composition was dominated by organics (80%), as has been previously reported (Coggon et al., 2014; Hersey et al., 2009; Sorooshian et al., 2007; Sorooshian, Ng, et al., 2007; Wang et al., 2008). A second, distinct factor displayed large mass loadings (up to 8 μg m^{-3}) within the AC-OAL (Figure S6) (O:C = 0.76), and the mass ratio of the AC-OAL to the MBL PMF factor is used as a tracer of AC-OAL entrainment into the MBL, as discussed in section 3.3.2. Possible aerosol production mechanisms in the AC-OAL include oxidation and transport of biogenic volatile organic compounds emitted by forested regions in the northwest United States, cloud droplet evaporation, and oxidation of sparingly soluble organics vented through the stratocumulus layer (Coggon et al., 2014; Heald et al., 2005; Sorooshian, Lu, et al., 2007). While large eddy simulations (LES) have demonstrated that the altitude of the top of the stratocumulus cloud deck can undergo diurnal variations of 10–100 m, providing a potential mechanism for AC-OAL aerosol production through droplet evaporation (Chen et al., 2011; Sorooshian, Lu, et al., 2007), the substantially larger mass fraction of organic aerosol in the AC-OAL than the MBL suggests that particle production is primarily a result of continental biogenic sources (Coggon et al., 2014). Observed aerosol mass loadings in the FT were the lowest sampled (1.5 μg m^{-3}) but agree well with previous aircraft measurements by Wang et al. (2008) off the coast of Pt. Reyes, CA, at a similar time of year (June–July).

3.2. Overview of Observed Aerosol Hygroscopicity

Figure 3 displays median aerosol number size distributions, κ_{AMS}, and κ_{CCN} values observed within the MBL, AC-OAL, and FT during each flight. For these comparisons, κ_{AMS} values are calculated assuming $\kappa_{org} = 0.1$, as is typical for non-urban regions (Mei et al., 2013; Moore et al., 2011, 2012). However, we note that using the parameterization developed by Lambe et al. (2011), the calculated κ_{org} values for the MBL and AC-OAL PMF factors are 0.19 and 0.17, respectively, due to their highly oxidized nature (Figure S6), suggesting the true κ_{org} values for large particles may be greater than 0.1.

Within the MBL, observed hygroscopicity values appear to cluster into three relatively distinct groups that span the range of values previously observed in this environment (Roberts et al., 2010; Royalty et al., 2017; Yakobi-Hancock et al., 2014). The strong temporal variation observed in both particle number size distributions and hygroscopicities underscores the complexity involved in accurately modeling CCN in coastal environments influenced by continental and marine sources. This is further demonstrated in Table 4, which depicts estimated organic and inorganic volume fractions of Aitken mode particles derived from MBL κ_{CCN} values. Assuming inorganic aerosol is entirely ammonium sulfate for these calculations, estimated organic fractions vary from effectively zero, as median κ_{CCN} during RF13 are larger than that of ammonium sulfate ($\kappa = 0.61$) to as high as 84%. The low hygroscopicities and subsequently large estimated organic fractions observed during flights RF9 and RF15 are uncharacteristic of remote marine environments and imply a continental influence on particle characteristics. κ_{AMS} values calculated during these flights are ~50–100% larger than κ_{CCN} values, implying addition of particle mass during growth that is more hygroscopic than the Aitken mode particles. While the difference between κ_{AMS} and κ_{CCN} values during these flights are nearly within the uncertainty range of the κ_{CCN} calculation, these observations align with those in many continental locations, where addition of inorganic mass to organic-rich Aitken mode particles growth is thought to lead to a positive relationship between particle hygroscopicity and size (Ervens et al., 2010; Kawana et al., 2016; Levin et al., 2014; Moore et al., 2012; Rose et al., 2011). On the other hand, κ_{AMS} and κ_{CCN} are quite similar during the other five flights, with relative deviations on the order of ~25% or less, which is well within the uncertainty of the κ_{CCN} measurements. A compilation of data reported by Royalty et al. (2017) suggests that minor variation of particle hygroscopicity with size is a common feature of remote marine aerosol, which generally exhibits elevated Aitken mode hygroscopicity. Four individual flights (RF4, RF5, RF13, and RF15) provide specific insight into the combined roles of aerosol sources and meteorological processes in determining aerosol hygroscopicity in the MBL, and these are discussed in further detail in section 3.3.2.

Within the AC-OAL, observed aerosol hygroscopicity is remarkably similar from flight-to-flight, and little difference is observed between κ_{CCN} and κ_{AMS} values. The combination of reduced hygroscopicity (i.e., κ ~0.2) and little variation with particle size suggests that within the AC-OAL, Aitken mode particles are organic-rich and grow through condensation of additional organic vapors, rather than addition of inorganic mass. Even under the assumption that the organic species in Aitken mode AC-OAL particles are entirely insoluble, total particle volume must be at least 66% organic to produce a hygroscopicity of 0.2

(assuming ammonium sulfate as the inorganic component). Chamber studies of monoterpene aerosol often observe κ_{org} of ~0.1–0.15 for Aitken mode particles (Alfarra et al., 2013; Zhao et al., 2015), which increases the estimated organic volume fraction to 80–89%. While the peak in the AC-OAL size distribution varies considerably between flights, the presence of a dominant Aitken mode in three out of four observations suggests particle formation may have occurred recently.

Coggon et al. (2014) first demonstrated that expansive dry air masses originating over the northwestern United States loft biogenic organic aerosol over the MBL and act as the main particle source to the AC-OAL. Our measurements support this conclusion; however, an additional contribution from organic gases vented through the stratocumulus layer cannot be ruled out. Comparing AC-OAL and MBL Aitken mode hygroscopicity suggests cloud droplet evaporation is at most a minor particle source to the AC-OAL, as during three of the four flights in which the AC-OAL was sampled, average MBL Aitken mode particles were substantially more hygroscopic than those in the AC-OAL (κ_{MBL} ~0.4; $\kappa_{AC\text{-}OAL}$ ~0.2). As the most hygroscopic particles in an air mass are likely to activate into cloud droplets, and as addition of inorganic mass is common during cloud processing in marine environments (Faloona, 2009; Seinfeld et al., 2016), it is unlikely that residual aerosol formed from evaporated cloud droplets would be less hygroscopic than the MBL aerosol population. Observations during RF15, discussed further in section 3.3.2, suggest entrainment during precipitation events can lead to a major AC-OAL signature in the MBL, directly demonstrating the importance of understanding the source of these particles.

Due to the low aerosol number concentrations in the FT, observed κ_{CCN} values vary widely between flights and exhibit large variability within individual flights. As a result, we hesitate to draw definitive conclusions based on these data. Other than RF13, average κ_{AMS} values from each flight are near or below 0.4, implying a substantial organic contribution to free tropospheric aerosol. In the absence of continental influence, observation of aerosols of such low hygroscopicity is unexpected, given that particle formation in the upper FT over tropical oceans is driven primarily by sulfuric acid nucleation and growth (Clarke, 1993; Clarke et al., 1998, 1999, 2013). Long range transport of organic aerosol layers from the Asian continent have been noted previously (Roberts et al., 2006, 2010), but estimates of aerosol hygroscopicity in such layers have varied dramatically. For instance, during the CIFEX experiments (Roberts et al., 2006), average κ attributed to aged aerosol layers were only ~0.04, whereas our measurements suggest a more moderate value of ~0.4, while observations by Roberts et al. (2010) indicated a value of 0.93 was more appropriate. While the substantial difference in particle concentrations in the MBL and FT observed during this campaign suggests FT aerosol plays a minor role in dictating MBL CCN activity on average, in remote marine environments, entrainment from the FT is the dominant source of MBL particles (Clarke, 1993; Clarke et al., 1996, 1998, 2013; Raes, 1995), and as such further research into the variability of FT aerosol composition is warranted.

3.3. Observation of Distinct Influences on MBL Particle Characteristics

Observations shown in Figure 3 indicate highly variable flight-averaged hygroscopicities in the MBL, suggesting that temporal variations in regional meteorology and/or particle source

strengths can strongly influence CCN characteristics in this environment. Further analysis suggests that in four of the seven flights discussed in this study, specific meteorological patterns and emissions sources influencing particle characteristics can be identified. We discuss these observations to provide insight into the level of physicochemical detail (both in terms of emissions and atmospheric dynamics) required for atmospheric models to simulate MBL CCN concentrations with high fidelity.

3.3.1. Shipping Emissions—Aerosol properties measured during RF4 and RF5 suggest a prominent influence of regional shipping emissions on particle characteristics and hygroscopicity in this environment. During these flights, the dominance of an Aitken mode near ~50–60 nm with much larger concentrations than in the FT suggests relatively recent formation from an MBL-based particle source. While such size distributions could hypothetically result from continental outflow (Moore et al., 2012), air mass backward trajectories remained over the ocean and near or within the MBL (<1,000 m) for the previous 5 days (Figure 4). Furthermore, trajectories transited primarily within the major shipping corridor along the coast, as observed for flights "perturbed" by shipping vessel emissions by Coggon et al. (2012), rather than recently arriving from the remote ocean (e.g., RF13). Downward mixing of AC-OAL particles is also ruled out as an Aitken mode particle source during these flights due to the distinctly different hygroscopicities observed in the MBL and AC-OAL (Figure 3). Finally, average wind speeds within the MBL were ~12 m s^{-1} and ~9 m s^{-1} during RF4 and RF5, respectively. Modini et al. (2015) previously noted that primary sea spray emissions produced particle concentrations of only 12 cm^{-3} during periods with similar windspeeds (12 m s^{-1}) in the same marine environment (equivalent to ~2% of particle number concentrations in the MBL during RF4 and RF5).

Shipping emissions have been previously noted as major contributors to aerosol and cloud properties in the N.E. Pacific environment (Cappa et al., 2014; Coggon et al., 2012; Lack et al., 2011; Murphy et al., 2009). Coggon et al. (2012) demonstrated that 70% of cloud residual particles measured in the California shipping lanes were impacted by nearby shipping emissions. Available compositional data further suggest that shipping emissions could be expected to produce Aitken mode hygroscopicities observed during RF4 and RF5. For instance, Lack et al. (2011) observed an effective κ value of 0.68–0.73 from exhaust produced by a large (96,500 ton) container vessel, while the smaller Research Vessel Atlantis sampled during the same study produced a value of ~0.2. Hygroscopic growth factor measurements of shipping exhaust emitted by another large (90,000 ton) container vessel by Murphy et al. (2009) suggest an effective $\kappa = 0.1–0.5$.

Direct measurements of a large container vessel exhaust plume during RF7 provide further support for the attribution of aerosol characteristics to shipping emissions in RF4 and RF5. As shown in Figure 5, the strong Aitken mode peak in the size distribution measured directly within the plume aligns well with those measured in RF4 and RF5, while the total magnitude of the flight-median size distributions agree well with those measured in the diluted plume more than 20 km downwind. As the plume was relatively narrow directly behind the ship, κ_{CCN} values are not available, but κ_{AMS} measurements agree well with those in RF4 and RF5 (Figure 5c). However, given the variability in the measured κ values of particulate shipping exhaust just discussed, this agreement cannot be viewed as definitive.

Ultimately, while the insights provided by the size distributions, backward trajectories, and κ_{AMS} values would not be definitive on their own, taken together they support a shipping emission signature on aerosol characteristics during these flights. This influence highlights the importance of accurate physicochemical representation of shipping vessel emissions within the California coastal zone. As an example, the implementation of recent regulations on the sulfur content of shipping fuel within coastal waters of the United States (up to 200 miles off the coast) should increase the organic:inorganic ratio of particulate shipping emissions in major shipping lanes over time (Cappa et al., 2014; Lack et al., 2011). Assuming, as a strictly upper limit estimate, that all Aitken mode particles observed during RF4 and RF5 are derived from shipping vessel emissions, changing the assumed hygroscopicity of these emissions from the value observed during ambient measurements in this study (~0.4–0.5) to a value of 0.1 (purely organic, partially hygroscopic), would change the CCN concentration at SS = 0.3% by 15–36%.

3.3.2. Entrainment From the AC-OAL—The observation of a single, dominant Aitken mode with reduced hygroscopicity during RF15 suggests an influence of the AC-OAL on MBL particle properties. According to Figure 4, the air mass sampled during RF15 had not recently transited over the continent or within the FT, which has previously shown to occasionally contain distinct layers of reduced hygroscopicity aerosol (Roberts et al., 2006, 2010). Clear evidence of entrainment from the AC-OAL is provided in Figure 6, which contrasts size distributions and κ_{AMS} values observed during RF15 and RF4, another flight with a prominent Aitken particle mode and relatively similar backward trajectory. During RF15, the MBL and AC-OAL size distributions are remarkably similar, exhibiting peak diameters at ~55 nm and lacking a larger accumulation mode. Liquid water contents measured within the MBL during RF15 demonstrate a fully developed stratocumulus layer encompassing roughly half of the MBL. κ_{AMS} values vary linearly with altitude from ~0.4 near the ocean surface to ~0.15–0.2 at the top of the cloud layer, aligning with the hypothesis of downward mixing of AC-OAL particles into the MBL. These observations are in stark contrast to those from RF4, where the Aitken mode diameter of the MBL and AC-OAL aerosol differ by ~20–25 nm, and importantly, the Aitken mode diameter in the MBL is smaller than the AC-OAL, suggesting a distinct particle source in each location. Finally, as the AC-OAL and MBL PMF factors are clearly distinguished in each flight where the AC-OAL layer was observed, the AC-OAL: MBL PMF factor mass ratio acts as a tracer for entrainment mixing. During RF15, the median AC-OAL: MBL PMF factor mass ratio was 0.81 in the MBL, in contrast to a value of 0.36 measured during RF4 and a median value of 0.42 in all flights other than RF15 where the AC-OAL was observed. The information obtained from the aerosol size distribution (no accumulation mode) and hygroscopicity (similar to the AC-OAL) in the MBL suggests that the distinct AC-OAL signature may result from entrainment following precipitation scavenging of the preexisting MBL aerosol. As typical AC-OAL particle concentrations are ~5 times as large as those in the overlying FT, failure to simulate this layer will result in underprediction of MBL particle concentrations during such distinct precipitation/entrainment events.

3.3.3. Transport From the Remote Pacific Ocean—Hygroscopicity measurements made during RF13 are notably larger than those from the other six flights, indicating a lack

of organic aerosol across the particle size distribution. As expected, backward trajectories calculated within the MBL during this flight indicate recent arrival from the remote Pacific Ocean, rather than extended transport through the major shipping lanes along the coast. The boundary layer was substantially compressed (<300 m) and cloud-free during the flight, suggesting ongoing subsidence of free tropospheric air masses (Figure 7a). As new particle formation through sulfuric acid nucleation is known to be a notable source of CCN throughout the marine boundary layer (Clarke, 1993; Clarke et al., 1998, 2013), downwelling and entrainment of such nucleated particles is a possible explanation for the elevated Aitken mode hygroscopicities observed. While low number concentrations in the FT make κ_{CCN} estimates less reliable, the values observed in RF13 are relatively similar to those in the MBL, supporting entrainment. While aerosol size distribution measurements in the FT suggest such entrainment was not responsible for increases in Aitken mode particles locally, as concentrations directly above the MBL are substantially lower than those in the MBL, the elevated aerosol concentrations at ~1,000 m suggest entrainment may have produced MBL Aitken mode particles during transport (Figure 7b). Furthermore, the vertical profile of the aerosol size distribution in the FT is consistent with past observations of growth of nucleation-produced Aitken mode particles during large-scale subsidence (Clarke et al., 1999).

Due to the compressed height of the MBL during RF13, the potential contribution of primary sea spray aerosol to MBL particle characteristics is also enhanced. However, using the size distribution fitting technique established by Modini et al. (2015), the calculated concentration of primary sea spray aerosol is only 18 cm^{-3} or ~4% of the average MBL particle concentration during the flight, suggesting sea spray provides at most a minor contribution.

3.4. CCN Closure Analysis

Figure 8 shows CCN closure results for the three sampled environments using six different assumptions regarding aerosol composition and mixing state. Three cases assume internally mixed aerosol components with composition determined by AMS measurements. These cases are differentiated by their assumptions regarding organic aerosol hygroscopicity, with κ_{org} increasing from 0 (first case), to 0.1 (second case), and finally to values predicted from time-varying measured OA O:C ratios according to the relationship developed by Lambe et al. (2011) (third case). The final three cases are similar to the internally mixed cases in their treatment of κ_{org}; however, the organic and inorganic aerosol components are assumed to be externally mixed. Bulk aerosol mass loadings were too low to obtain robust estimates of size-resolved composition, precluding more detailed treatment of composition in CCN closure calculations. Closure was assessed in terms of the normalized mean bias ($NMB = \sum (CCN_{pred,i} - CCN_{meas,i}) / \sum CCN_{meas}$), similarly to Asa-Awuku et al. (2011), which provides a representation of the average CCN prediction error observed for each flight. Data for the MBL and FT are shown for individual flights, while data from the AC-OAL are aggregated from all flights where the layer was observed, as fewer size distributions were obtained from the AC-OAL during each flight (and the AC-OAL was not observed at all during three flights).

For the majority of analyzed flights (five out of seven), closure is obtained within 20% using AMS-measured bulk composition and an assumption of either insoluble ($\kappa_{org} = 0$) or slightly hygroscopic organics ($\kappa_{org} = 0.1$). While the assumption of insoluble organics disagrees with observed O:C ratios (e.g., the O:C ratio of the MBL PMF factor is 0.85), CCN closure studies often find this assumption is ideal when assuming internal mixing (Chang et al., 2007; Lance et al., 2009; Moore et al., 2011; Wang et al., 2008). The lack of strong dependence on κ_{org} suggests that in non-urban areas, regional models may be able to assign a single value to organic aerosol rather than attempt to dynamically model changes in organic aerosol hygroscopicity with aging (Wang et al., 2008). This is further highlighted by the fact that closure results assuming a constant κ org value (0.1) are generally more accurate than those produced by parameterizing κ_{org} based on the observed O:C ratio (Lambe et al., 2011). As larger aerosols are more likely to have undergone cloud-processing, parameterizing organic hygroscopicity based on bulk measurements of the organic O:C ratio, which is biased by the largest particles, may also overpredict the oxidation state of particles near the critical diameter of CCN activation. Without size-resolved compositional data, it is difficult to definitively conclude whether the overprediction observed when κ_{org} is parameterized based on the organic O:C ratio is due to such variability with size or is the result of a different relationship between O:C and κ_{org} for organic aerosols in this environment. However, other published parameterizations between O:C and κ_{org} in the literature either agree well with the Lambe parameterization (Chang et al., 2010; Massoli et al., 2010; Thalman et al., 2017) or predict more hygroscopic particles at the same O:C ratio (and as a result would lead to further overprediction if implemented in the CCN closure analysis) (Mei et al., 2013). The overprediction in CCN observed here when incorporating the Lambe parameterization therefore suggests that small particles near the critical activation diameter are less hygroscopic than larger particles that dominate the mass size distribution and thereby dictate AMS-measured composition.

Overall, generally good closure is expected in a semi-remote environment such as the California coastal zone, as previous studies have noted that closure is likely to be achieved within 20% when the bulk aerosol κ exceeds 0.1 (Wang et al., 2010). Furthermore, it is expected that aerosol in this coastal environment can be modeled as internally mixed, regardless of its true mixing state, due to the substantial contribution of inorganic constituents and distance from emission sources (Ervens et al., 2010; Fierce et al., 2016; Moore et al., 2012). Fierce et al. (2016) have demonstrated that in semi-remote environments (i.e., non-urban locations), initially externally mixed aerosol becomes internally mixed on a time scale of about 1 day, while the conversion is even faster (on the order of hours) in urban environments, in agreement with the results of Wang et al. (2010). Notable underpredictions (i.e., >20%) of CCN concentrations are produced when assuming externally mixed aerosol with insoluble organics, in agreement with the aged nature of the aerosol in this environment, which should lead to both oxidized organic aerosol and an appreciable amount of internal mixing.

CCN are strongly overpredicted in the MBL during RF9 (37%) and RF15 (57%) when assuming an internal mixture with hygroscopic organics. Aerosol composition during these flights was dominated by organic species in the MBL (59% and 58% of AMS-derived aerosol mass, respectively), indicative of a continental influence on aerosol properties.

AMS-derived hygroscopicities are substantially larger than those derived from CCN measurements (Figure 3), suggesting that size-dependent composition may lead to the observed overprediction of CCN concentrations when using bulk AMS measurements of aerosol composition. Comparison of CCN closure results when assuming internal versus external mixing suggests that organic and inorganic components are externally mixed, implying either distinct particle sources or a lack of significant aging prior to measurement. In the case of RF15, this external mixing aligns with the hypothesis of downward mixing from the organic-rich AC-OAL. Figure S7 depicts the CCN closure normalized mean bias resulting from an assumption of internally mixed aerosols with hygroscopic organics as a function of the CCN-derived hygroscopicity. In general, CCN closure error increases rapidly as κ_{CCN} decreases past ~0.25, suggesting that detailed mixing state and/or size resolved compositional information is critical for accurate CCN prediction in this coastal environment during periods of intense organic aerosol intrusion into the MBL. As the aerosol hygroscopicity calculation used in this study relies on an assumption of internal mixing of organic and inorganic aerosol components, it is difficult to determine whether CCN closure error when assuming internal mixing during this flights is a result of externally mixed organic and inorganic aerosol or a result of variable composition with size. Ultimately, as these atypical organic aerosol-dominated marine conditions are the least likely to be accurately reproduced by regional models, further investigation of their frequency, particle characteristics, and resulting impact on cloud properties is warranted.

The analysis presented in Figure 8 implies that for typical conditions in the MBL (5 out of 7 flights in this study), mixing state and organic hygroscopicity have relatively little influence on CCN number concentrations. Additional closure analyses were performed assuming a constant κ equivalent to values attributed to average continental ($\kappa = 0.27$) and marine ($\kappa = 0.72$) environments (Pringle et al., 2010) (Figure 9). These results highlight the fact that assuming coastal aerosols have a strictly marine character leads to substantial errors in CCN prediction (>20% for 8 out of 9 flights) even if size distribution parameters are well characterized. Furthermore, for five out of the seven analyzed flights (RF4, RF5, RF9, RF13, RF16), assuming a constant marine κ (0.72) results in CCN prediction error similar to or larger than the error produced by assuming a constant aerosol size distribution derived from the median value measured in the MBL during this study. This underscores the importance of capturing organic contributions to coastal MBL aerosol, whether due to continental outflow, downwelling from the AC-OAL, shipping emissions, or marine biota.

3.5. Sensitivity of Stratocumulus CDNC to Below-Cloud Aerosol Hygroscopicity

In order to directly investigate the sensitivity of N.E. Pacific stratocumulus CDNC to below-cloud aerosol properties, droplet activation was simulated using an aerosol-cloud parcel model constrained with detailed below-cloud aerosol measurements obtained from three cloud sampling passes performed during the campaign. While a number of previous cloud parcel modeling studies have assumed unimodal size distributions (Chen et al., 2016; Reutter et al., 2009 ; Ward et al., 2010), observed aerosol size distributions over the N.E. Pacific were frequently bimodal (Figure 3). As many current aerosol modules incorporated within global atmospheric chemistry models involve multiple aerosol size modes (Liu & Wang, 2010; Pringle et al., 2010; Rothenberg et al., 2018), we carried out parcel model runs

to analyze CDNC sensitivity to properties of the Aitken and accumulation modes separately. Sensitivities were calculated following McFiggans et al. (2006), where $S(X_i) = \delta lnN_{CDNC}/\delta lnX_i$ and X_i is the parameter under investigation. Standard linear regressions of lnN_{CDNC} versus lnX_i were used to determine $S(X_i)$ values, as is convention (Reutter et al., 2009; Sánchez-Gácita et al., 2017; Ward et al., 2010). Measured aerosol and meteorological properties utilized as model constraints are summarized in Table 5. Sensitivity to hygroscopicity was computed across the range of $\kappa = 0.2–0.6$. Initial results confirmed that for observed MSc updraft velocities ($w = 0.15–0.3$ m s^{-1}), below-cloud particle number concentrations (~500–800 cm^{-3}), and typical hygroscopicities ($\kappa \sim 0.2–0.4$), properties of the Aitken mode have a minor impact on stratocumulus properties ($S(X_i) < 0.05$), as minimum simulated activation diameters exceed 100 nm. Therefore, Figure 10 depicts the sensitivity of stratocumulus CDNC to properties of the accumulation mode and the simulated updraft velocity.

The average sensitivity of CDNC to aerosol hygroscopicity (0.19), while smaller than the sensitivity to size distribution parameters, is 39% as large as the sensitivity to the geometric mean diameter of the accumulation mode. This agrees with the consensus that particle size distribution properties have a larger influence on CCN concentration than particle composition (Dusek et al., 2006; McFiggans et al., 2006; Reutter et al., 2009), but also suggests accurate hygroscopicity reproduction should be included in future model improvement efforts. Observed below-cloud particle number concentrations and updraft velocities suggest that CCN activation occurs in the transitional regime according to the designations defined by Reutter et al. (2009), and simulated sensitivity to hygroscopicity agrees well with those previously reported for the transition regime (0.17–0.2) (Reutter et al., 2009; Ward et al., 2010).

Aging processes during transport likely lead to internally rather than externally mixed aerosol in the MBL. The simulated error in predicted CDNC when assuming fully externally mixed components is only 7.6–8.7% for the three modeled cases. This aligns with the observation of similarly accurate CCN closure results for the MBL when assuming internally or externally mixed components and a κ_{org} of 0.1 or larger. As the volume fraction of inorganic aerosol in the accumulation mode is likely to increase with increasing distance from the coast, this predicted mixing-state-related error may be an upper bound for marine conditions in general.

Previous aerosol-cloud parcel modeling studies have demonstrated that the sensitivity of predicted CDNC to aerosol hygroscopicity tends to decrease as bulk hygroscopicity increases, especially for the aerosol-limited and transitional aerosol activation regimes (Reutter et al., 2009; Sánchez-Gácita et al., 2017). If this is the case, accurate hygroscopicity characterization in marine regions subject to organic aerosol inputs, which contain aerosol with lower-than-average κ values, may be more important for global CDNC prediction accuracy than accurate hygroscopicity characterization in remote regions subject to aerosol sources with different, but elevated, hygroscopicities (e.g., ammonium sulfate [$\kappa = 0.61$] vs. sodium chloride [$\kappa = 1.28$]). To investigate this possibility, we calculated local CDNC sensitivity to aerosol hygroscopicity for four hypothetical marine aerosol size distributions. Rather than performing a linear regression on data obtained from a broad range of

hygroscopicities, as was done for the data shown in Figure 10, local sensitivities refer to calculations performed on incremental variations in κ (e.g., $\kappa = 0.1$ vs. 0.2). Figure 11 displays the size distributions used as well as the sensitivity results. In order to span the likely range of size distributions observed in marine environments, the "Coastal" distribution is similar to median distributions observed during RF4 and RF5. A "Remote" distribution was generated using reported size distribution parameters from measurements over the remote subtropical N. Pacific by Ueda et al. (2016). Two additional size distributions were produced by interpolating between the "Coastal" and "Remote" distributions. Total particle concentrations in the simulations varied between 300 and 800 cm^{-3} depending on the size distribution used. Five different updraft velocities were simulated ($w = 0.1–0.5$ m s^{-1}), corresponding to the range typically observed within MSc over the Pacific (Zheng et al., 2016).

A few notable trends are evident in the results shown in Figure 11. As has been previously reported, CDNC sensitivity to aerosol hygroscopicity tends to decrease as hygroscopicity increases. However, even at low hygroscopicities, calculated sensitivities never exceed 0.3, suggesting that at a maximum, a 50% error in marine aerosol hygroscopicity should lead to an error of only 15% in predicted CDNC. Sensitivity slightly increases as the assumed particle concentration increases, and therefore, hygroscopicity is slightly less important in remote marine environments than in more polluted, coastal locations, as expected. In typical remote marine conditions ($\kappa \approx 0.6$) for instance, a 50% error in hygroscopicity is associated with only a ~2.5–7.5% error in predicted CDNC, while in coastal environments ($\kappa \approx 0.35$) the error is estimated to be ~7.5–15%.

When simulating certain combinations of updraft velocity and aerosol size distribution, the sensitivity of predicted CDNC to aerosol hygroscopicity does not decrease monotonically as hygroscopicity increases. Furthermore, at a given hygroscopicity value shown in Figure 11, CDNC sensitivity is a non-monotonic function of updraft velocity. Here, we demonstrate that these phenomena are a result of activation of the distinct Aitken aerosol mode. Variation in CDNC sensitivity to hygroscopicity with increasing updraft velocity is shown in Figure 12 for $\kappa = 0.6–0.8$. Local CDNC sensitivity to hygroscopicity initially decreases with increasing updraft velocity before increasing again at updraft velocities >0.2–0.3 m s^{-1}. This trend is consistent regardless of κ range analyzed; however, the shape of the curve becomes "stretched" horizontally as κ values decrease (Figure 12). Using a unimodal size distribution, Reutter et al. (2009) demonstrated that moving from the transitional to the aerosol-limited regime caused CDNC sensitivity to hygroscopicity to decline for all $\kappa >$ 0.05. For the four marine size distributions simulated in this study, increasing the updraft velocity from 0.1 to 1.0 m s^{-1} shifts activation from the transitional regime to the aerosol-limited regime, implying CDNC sensitivity to hygroscopicity should subsequently decline. Our observation of the opposite phenomenon is due to the fact that at low ($w = 0.1$ m s^{-1}) and high ($w = 1–1.5$ m s^{-1}) updraft velocities, critical diameters produced within the rising air parcel occur near the peak of the accumulation and Aitken aerosol modes, respectively (Figure 12b). As the size distribution is peaked at these locations, subtle changes in aerosol hygroscopicity that induce small changes in the critical diameter result in a relatively large change in computed CDNC—hence elevated sensitivity to hygroscopicity. In contrast, for moderate ($w \sim 0.2–0.3$ m s^{-1}) updraft velocities, minimum critical diameters occur between

the peaks of the Aitken and accumulation modes, and for very strong updraft velocities ($w >$ 1.5–2 m s^{-1}) minimum critical diameters occur at sizes smaller than the peak of the Aitken mode, leading to lowered sensitivity (Figure 12b). This implies that in aerosol-limited environments with bimodal aerosol size distributions, the sensitivity of CDNC to hygroscopicity cannot necessarily be assumed to be negligible based solely on the ratio of the updraft velocity to particle number concentration. Ultimately, our results suggest that the sensitivity of marine CDNC to hygroscopicity is maximized in weak updraft conditions occurring in MSc ($w < 0.2$ m s^{-1}), where hygroscopicity of the accumulation, rather than the Aitken, mode is most relevant to accurate CDNC prediction, and in relatively strong updraft conditions ($0.5 < w < 2$ m s^{-1}) in either MSc or marine cumulus (Clarke et al., 1996), where Aitken mode hygroscopicity has a larger influence on CDNC than that of the accumulation mode.

4. Summary and Conclusions

Measurements of aerosol properties obtained over the N.E. Pacific Ocean during the MACAWS campaign in June and July 2018 were combined with results from an aerosol-cloud-parcel model to gain insight into aerosol hygroscopicity and its influence on CCN and MSc CDNC prediction in this environment. Three characteristic vertical regions were characterized, corresponding to the MBL, FT, and AC-OAL. Within the MBL, flight-averaged hygroscopicities varied from values typical of continental environments ($\kappa = 0.27$), to those representative of remote marine locations ($\kappa = 0.72$) (Pringle et al., 2010). Distinct influences on MBL particle characteristics, including shipping emissions, entrainment from the AC-OAL, and transport from the remote Pacific, were identified through analysis of hygroscopicity data. In the AC-OAL, observed hygroscopicity suggests a dominant contribution of organic aerosol in both the Aitken and accumulation mode size ranges.

For the majority of flights, measured CCN concentrations could be reproduced within 20% using measurements of the aerosol size distribution, bulk hygroscopicity, and an assumption of either internally or externally mixed organic and inorganic components, in agreement with past results in non-urban locations (e.g., Ervens et al., 2010). Notably, for five of the seven flights, MBL CCN were better predicted when assuming a constant aerosol number size distribution derived from the median value measured in the MBL than when assuming a constant κ typical of remote marine locations (0.72).

Results from an aerosol-cloud-parcel model confirm that the sensitivity ($S(Xi) = \delta lnN_{CDNC}/\delta lnX_i$) of predicted CDNC to accumulation mode aerosol hygroscopicity (0.19) is substantially smaller than sensitivity to size distribution parameters, such as the accumulation mode geometric diameter (0.49) and standard deviation (−0.64). Simulations using a variety of possible MBL aerosol size distributions and hygroscopicities suggest that a 50% error in predicted hygroscopicity should rarely produce a CDNC error greater than 15%. However, model results further suggest that CDNC sensitivity to hygroscopicity does not monotonically decrease with increasing updraft velocity. Rather, sensitivity appears to decrease or remain constant with increasing updraft velocities from low to moderate values (e.g., 0.1–0.3 m s^{-1}) and then increase as updraft velocities increase further (>0.4 m s^{-1}) due to activation of the distinct Aitken mode of the aerosol size distribution. This phenomenon is

observed despite the fact that at large updraft velocities (>0.4–0.5 m s^{-1}), marine conditions generally occupy the aerosol-limited regime of cloud droplet activation. Ultimately, CDNC sensitivity to hygroscopicity is predicted to be maximized in weak updraft conditions occurring in MSc (<0.2 m s^{-1}) and in strong updraft conditions (>0.5 m s^{-1}) expected to occur in either MSc or marine cumulus.

Supplementary Material

Refer to Web version on PubMed Central for supplementary material.

Acknowledgments

This work was supported by Office of Naval Research Grants N00014-17-1-2719 and N00014-16-1-2567. AS was partially supported by NASA Grant 80NSSC19K0442 in support of the ACTIVATE Earth Venture Suborbital-3 (EVS-3) investigation, which is funded by NASA's Earth Science Division and managed through the Earth System Science Pathfinder Program Office. We would like to thank the crew of the CIRPAS Twin Otter for their assistance during the campaign.

References

Ackerman AS, Toon OB, & Hobbs PV (1993). Dissipation of marine stratiform clouds and collapse of the marine boundary layer due to the depletion of cloud condensation nuclei by clouds. Science, 262(5131), 226–229. 10.1126/science.262.5131.226 [PubMed: 17841869]

Albrecht BA (1989). Aerosols, cloud microphysics, and fractional cloudiness. Science, 245(4923), 1227–1230. 10.1126/science.245.4923.1227 [PubMed: 17747885]

Alfarra MR, Good N, Wyche KP, Hamilton JF, Monks PS, Lewis AC, & McFiggans G (2013). Water uptake is independent of the inferred composition of secondary aerosols derived from multiple biogenic VOCs. Atmospheric Chemistry and Physics, 13(23), 11,769–11,789. 10.5194/acp-13-11769-2013

Almeida GP, Brito J, Morales CA, Andrade MF, & Artaxo P (2014). Measured and modelled cloud condensation nuclei (CCN) concentration in São Paulo, Brazil: The importance of aerosol size-resolved chemical composition on CCN concentration prediction. Atmospheric Chemistry and Physics, 14(14), 7559–7572. 10.5194/acp-14-7559-2014

Andreae MO, & Rosenfeld D (2008). Aerosol-cloud-precipitation interactions. Part 1. The nature and sources of cloud-active aerosols. Earth-Science Reviews, 89(1), 13–41. 10.1016/j.earscirev.2008.03.001

Asa-Awuku A, Moore RH, Nenes A, Bahreini R, Holloway JS, Brock CA, et al. (2011). Airborne cloud condensation nuclei measurements during the 2006 Texas Air Quality Study. Journal of Geophysical Research, 116, D11201 10.1029/2010JD014874

Asa-Awuku A, Nenes A, Gao S, Flagan RC, & Seinfeld JH (2010). Water-soluble SOA from alkene ozonolysis: Composition and droplet activation kinetics inferences from analysis of CCN activity. Atmospheric Chemistry and Physics, 10(4), 1585–1597. 10.5194/acp-10-1585-2010

Berner AH, Bretherton CS, & Wood R (2015). Large eddy simulation of ship tracks in the collapsed marine boundary layer: A case study from the Monterey area ship track experiment. Atmospheric Chemistry and Physics, 15(10), 5851–5871. 10.5194/acp-15-5851-2015

Bhattu D, & Tripathi SN (2015). CCN closure study: Effects of aerosol chemical composition and mixing state. Journal of Geophysical Research: Atmospheres, 120, 766–783. 10.1002/2014JD021978

Bougiatioti A, Nenes A, Fountoukis C, Kalivitis N, Pandis SN, & Mihalopoulos N (2011). Size-resolved CCN distributions and activation kinetics of aged continental and marine aerosol. Atmospheric Chemistry and Physics, 11(16), 8791–8808. 10.5194/acp-11-8791-2011

Brenguier J-L, Pawlowska H, Schüller L, Preusker R, Fischer J, & Fouquart Y (2000). Radiative properties of boundary layer clouds: Droplet effective radius versus number concentration. Journal

of the Atmospheric Sciences, 57(6), 803–821. 10.1175/1520-0469(2000)057<0803:RPOBLC>2.0.CO;2

Brioude J, Cooper OR, Feingold G, Trainer M, Freitas SR, Kowal D, et al. (2009). Effect of biomass burning on marine stratocumulus clouds off the California coast. Atmospheric Chemistry and Physics, 9(22), 8841–8856. 10.5194/acp-9-8841-2009

Canagaratna MR, Jimenez JL, Kroll JH, Chen Q, Kessler SH, Massoli P, et al. (2015). Elemental ratio measurements of organic compounds using aerosol mass spectrometry: Characterization, improved calibration, and implications. Atmospheric Chemistry and Physics, 15(1), 253–272. 10.5194/acp-15-253-2015

Cappa CD, Williams EJ, Lack DA, Buffaloe GM, Coffman D, Hayden KL, et al. (2014). A case study into the measurement of ship emissions from plume intercepts of the NOAA ship Miller Freeman. Atmospheric Chemistry and Physics, 14(3), 1337–1352. 10.5194/acp-14-1337-2014

Carman JK, Rossiter DL, Khelif D, Jonsson HH, Faloona IC, & Chuang PY (2012). Observational constraints on entrainment and the entrainment interface layer in stratocumulus. Atmospheric Chemistry and Physics, 12(22), 11,135–11,152. 10.5194/acp-12-11135-2012

Chang RY-W, Liu PSK, Leaitch WR, & Abbatt JPD (2007). Comparison between measured and predicted CCN concentrations at Egbert, Ontario: Focus on the organic aerosol fraction at a semi-rural site. Atmospheric Environment, 41(37), 8172–8182. 10.1016/j.atmosenv.2007.06.039

Chang RY-W, Slowik JG, Shantz NC, Vlasenko A, Liggio J, Sjostedt SJ, et al. (2010). The hygroscopicity parameter (κ) of ambient organic aerosol at a field site subject to biogenic and anthropogenic influences: Relationship to degree of aerosol oxidation. Atmospheric Chemistry and Physics, 10(11), 5047–5064. 10.5194/acp-10-5047-2010

Chen J, Liu Y, Zhang M, & Peng Y (2016). New understanding and quantification of the regime dependence of aerosol-cloud interaction for studying aerosol indirect effects. Geophysical Research Letters, 43, 1780–1787. 10.1002/2016GL067683

Chen Y-C, Xue L, Lebo ZJ, Wang H, Rasmussen RM, & Seinfeld JH (2011). A comprehensive numerical study of aerosol-cloud-precipitation interactions in marine stratocumulus. Atmospheric Chemistry and Physics, 11(18), 9749–9769. 10.5194/acp-11-9749-2011

Clarke AD (1993). Atmospheric nuclei in the Pacific midtroposphere: Their nature, concentration, and evolution. Journal of Geophysical Research, 98(D11), 20,633–20,647. 10.1029/93JD00797 [PubMed: 11539182]

Clarke AD, Eisele F, Kapustin VN, Moore K, Tanner D, Mauldin L, et al. (1999). Nucleation in the equatorial free troposphere: Favorable environments during PEM-Tropics. Journal of Geophysical Research, 104(D5), 5735–5744. 10.1029/98JD02303

Clarke AD, Freitag S, Simpson RMC, Hudson JG, Howell SG, Brekhovskikh VL, et al. (2013). Free troposphere as a major source of CCN for the equatorial pacific boundary layer: Long-range transport and teleconnections. Atmospheric Chemistry and Physics, 13(15), 7511–7529. 10.5194/acp-13-7511-2013

Clarke AD, Li Z, & Litchy M (1996). Aerosol dynamics in the equatorial Pacific marine boundary layer: Microphysics, diurnal cycles and entrainment. Geophysical Research Letters, 23(7), 733–736. 10.1029/96GL00778

Clarke AD, Varner JL, Eisele F, Mauldin RL, Tanner D, & Litchy M (1998). Particle production in the remote marine atmosphere: Cloud outflow and subsidence during ACE 1. Journal of Geophysical Research, 103(D13), 16,397–16,409. 10.1029/97JD02987

Coggon MM, Sorooshian A, Wang Z, Craven JS, Metcalf AR, Lin JJ, et al. (2014). Observations of continental biogenic impacts on marine aerosol and clouds off the coast of California. Journal of Geophysical Research: Atmospheres, 119, 6724–6748. 10.1002/2013JD021228

Coggon MM, Sorooshian A, Wang Z, Metcalf AR, Frossard AA, Lin JJ, et al. (2012). Ship impacts on the marine atmosphere: Insights into the contribution of shipping emissions to the properties of marine aerosol and clouds. Atmospheric Chemistry and Physics, 12(18), 8439–8458. 10.5194/acp-12-8439-2012

Collins DB, Ault AP, Moffet RC, Ruppel MJ, Cuadra-Rodriguez LA, Guasco TL, et al. (2013). Impact of marine biogeo-chemistry on the chemical mixing state and cloud forming ability of nascent sea

spray aerosol. Journal of Geophysical Research: Atmospheres, 118, 8553–8565. 10.1002/jgrd.50598

Cubison MJ, Ervens B, Feingold G, Docherty KS, Ulbrich IM, Shields L, et al. (2008). The influence of chemical composition and mixing state of Los Angeles urban aerosol on CCN number and cloud properties. Atmospheric Chemistry and Physics, 8(18), 5649–5667. 10.5194/acp-8-5649-2008

Dadashazar H, Braun RA, Crosbie E, Chuang PY, Woods RK, Jonsson HH, & Sorooshian A (2018). Aerosol characteristics in the entrainment interface layer in relation to the marine boundary layer and free troposphere. Atmospheric Chemistry and Physics, 18(3), 1495–1506. 10.5194/acp-18-1495-2018

DeCarlo PF, Kimmel JR, Trimborn A, Northway MJ, Jayne JT, Aiken AC, et al. (2006). Field-deployable, high-resolution, time-of-flight aerosol mass spectrometer. Analytical Chemistry, 78(24), 8281–8289. 10.1021/ac061249n [PubMed: 17165817]

Draxler RR, & Hess GD (1997). Description of the HYSPLIT_4 modeling system NOAA. Tech. Memo. ERL ARL-224 (pp. 1–24). Silver Spring: NOAA Air Resources Laboratory.

Draxler RR, & Hess GD (1998). An overview of the HYSPLIT_4 modelling system for trajectories, dispersion, and deposition. Australian Meteorological Magazine, 47, 295–308.

Duplissy J, DeCarlo PF, Dommen J, Alfarra MR, Metzger A, Barmpadimos I, et al. (2011). Relating hygroscopicity and composition of organic aerosol particulate matter. Atmospheric Chemistry and Physics, 11(3), 1155–1165. 10.5194/acp-11-1155-2011

Duplissy J, Gysel M, Alfarra MR, Dommen J, Metzger A, Prevot ASH, et al. (2008). Cloud forming potential of secondary organic aerosol under near atmospheric conditions. Geophysical Research Letters, 35, L03818 10.1029/2007GL031075

Dusek U, Frank GP, Hildebrandt L, Curtius J, Schneider J, Walter S, et al. (2006). Size matters more than chemistry for cloud-nucleating ability of aerosol particles. Science, 312(5778), 1375–1378. 10.1126/science.1125261 [PubMed: 16741120]

Ervens B, Cubison M, Andrews E, Feingold G, Ogren JA, Jimenez JL, et al. (2007). Prediction of cloud condensation nucleus number concentration using measurements of aerosol size distributions and composition and light scattering enhancement due to humidity. Journal of Geophysical Research, 112, D10S32 10.1029/2006JD007426

Ervens B, Cubison MJ, Andrews E, Feingold G, Ogren JA, Jimenez JL, et al. (2010). CCN predictions using simplified assumptions of organic aerosol composition and mixing state: A synthesis from six different locations. Atmospheric Chemistry and Physics, 10 (10), 4795–4807. 10.5194/acp-10-4795-2010

Faloona I (2009). Sulfur processing in the marine atmospheric boundary layer: A review and critical assessment of modeling uncertainties. Atmospheric Environment, 43(18), 2841–2854. 10.1016/j.atmosenv.2009.02.043

Fierce L, Riemer N, & Bond TC (2016). Toward reduced representation of mixing state for simulating aerosol effects on climate. Bulletin of the American Meteorological Society, 98(5), 971–980. 10.1175/BAMS-D-16-0028.1

Frosch M, Bilde M, Nenes A, Praplan AP, Jurányi Z, Dommen J, et al. (2013). CCN activity and volatility of β-caryophyllene secondary organic aerosol. Atmospheric Chemistry and Physics, 13(4), 2283–2297. 10.5194/acp-13-2283-2013

Gerber H, Arends BG, & Ackerman AS (1994). New microphysics sensor for aircraft use. Atmospheric Research, 31(4), 235–252. 10.1016/0169-8095(94)90001-9

Goren T, & Rosenfeld D (2012). Satellite observations of ship emission induced transitions from broken to closed cell marine stratocumulus over large areas. Journal of Geophysical Research, 117, D17206 10.1029/2012JD017981

Gunthe SS, King SM, Rose D, Chen Q, Roldin P, Farmer DK, et al. (2009). Cloud condensation nuclei in pristine tropical rainforest air of Amazonia: Size-resolved measurements and modeling of atmospheric aerosol composition and CCN activity. Atmospheric Chemistry and Physics, 9(19), 7551–7575. 10.5194/acp-9-7551-2009

Hallquist M, Wenger JC, Baltensperger U, Rudich Y, Simpson D, Claeys M, et al. (2009). The formation, properties and impact of secondary organic aerosol: Current and emerging issues. Atmospheric Chemistry and Physics, 9(14), 5155–5236. 10.5194/acp-9-5155-2009

Heald CL, Jacob DJ, Park RJ, Russell LM, Huebert BJ, Seinfeld JH, et al. (2005). A large organic aerosol source in the free troposphere missing from current models. Geophysical Research Letters, 32, L18809 10.1029/2005GL023831

Hegg DA, Covert DS, Jonsson H, & Covert PA (2005). Determination of the transmission efficiency of an aircraft aerosol inlet. Aerosol Science and Technology, 39(10), 966–971. 10.1080/02786820500377814

Hegg DA, Covert DS, Jonsson HH, & Woods RK (2010). The contribution of anthropogenic aerosols to aerosol light-scattering and CCN activity in the California coastal zone. Atmospheric Chemistry and Physics, 10(15), 7341–7351. 10.5194/acp-10-7341-2010

Hersey SP, Sorooshian A, Murphy SM, Flagan RC, & Seinfeld JH (2009). Aerosol hygroscopicity in the marine atmosphere: A closure study using high-time-resolution, multiple-RH DASH-SP and size-resolved C-ToF-AMS data. Atmospheric Chemistry and Physics, 9(7), 2543–2554. 10.5194/acp-9-2543-2009

Jimenez JL, Canagaratna MR, Donahue NM, Prevot ASH, Zhang Q, Kroll JH, et al. (2009). Evolution of organic aerosols in the atmosphere. Science, 326(5959), 1525–1529. 10.1126/science.1180353 [PubMed: 20007897]

Kanakidou M, Seinfeld JH, Pandis SN, Barnes I, Dentener FJ, Facchini MC, et al. (2005). Organic aerosol and global climate modelling: A review. Atmospheric Chemistry and Physics, 5(4), 1053–1123. 10.5194/acp-5-1053-2005

Kawana K, Nakayama T, & Mochida M (2016). Hygroscopicity and CCN activity of atmospheric aerosol particles and their relation to organics: Characteristics of urban aerosols in Nagoya, Japan. Journal of Geophysical Research: Atmospheres, 121, 4100–4121. 10.1002/2015JD023213

Köhler H (1936). The nucleus in and the growth of hygroscopic droplets. Transactions of the Faraday Society, 32(0), 1152–1161. 10.1039/TF9363201152

Kreidenweis SM, & Asa-Awuku A (2014). 5.13—Aerosol Hygroscopicity: Particle water content and its role in atmospheric processes In Holland HD, & Turekian KK (Eds.), Treatise on geochemistry (Second ed.pp. 331–361). Oxford: Elsevier 10.1016/B978-0-08-095975-7.00418-6

Lack DA, Cappa CD, Langridge J, Bahreini R, Buffaloe G, Brock C, et al. (2011). Impact of fuel quality regulation and speed reductions on shipping emissions: Implications for climate and air quality. Environmental Science & Technology, 45(20), 9052–9060. 10.1021/es2013424 [PubMed: 21910443]

Lambe AT, Onasch TB, Massoli P, Croasdale DR, Wright JP, Ahern AT, et al. (2011). Laboratory studies of the chemical composition and cloud condensation nuclei (CCN) activity of secondary organic aerosol (SOA) and oxidized primary organic aerosol (OPOA). Atmospheric Chemistry and Physics, 11(17), 8913–8928. 10.5194/acp-11-8913-2011

Lance S, Nenes A, Mazzoleni C, Dubey MK, Gates H, Varutbangkul V, et al. (2009). Cloud condensation nuclei activity, closure, and droplet growth kinetics of Houston aerosol during the Gulf of Mexico Atmospheric Composition and Climate Study (GoMACCS). Journal of Geophysical Research, 114, D00F15 10.1029/2008JD011699

Lance S, Nenes A, Medina J, & Smith JN (2006). Mapping the operation of the DMT continuous flow CCN counter. Aerosol Science and Technology, 40(4), 242–254. 10.1080/02786820500543290

Latham J, Rasch P, Chen C-C, Kettles L, Gadian A, Gettelman A, et al. (2008). Global temperature stabilization via controlled albedo enhancement of low-level maritime clouds. Philosophical Transactions of the Royal Society A: Mathematical, Physical and Engineering Sciences, 366(1882), 3969–3987. 10.1098/rsta.2008.0137

Levin EJT, Prenni AJ, Palm BB, Day DA, Campuzano-Jost P, Winkler PM, et al. (2014). Size-resolved aerosol composition and its link to hygroscopicity at a forested site in Colorado. Atmospheric Chemistry and Physics, 14(5), 2657–2667. 10.5194/acp-14-2657-2014

Liu X, & Wang J (2010). How important is organic aerosol hygroscopicity to aerosol indirect forcing? Environmental Research Letters, 5(4), 044010 10.1088/1748-9326/5/4/044010

MacDonald AB, Dadashazar H, Chuang PY, Crosbie E, Wang H, Wang Z, et al. (2018). Characteristic vertical profiles of cloud water composition in marine stratocumulus clouds and relationships with precipitation. Journal of Geophysical Research: Atmospheres, 123, 3704–3723. 10.1002/2017JD027900

Mardi AH, Dadashazar H, MacDonald AB, Braun RA, Crosbie E, Xian P, et al. (2018). Biomass burning plumes in the vicinity of the California coast: Airborne characterization of physicochemical properties, heating rates, and spatiotemporal features. Journal of Geophysical Research: Atmospheres, 123, 13,560–13,582. 10.1029/2018JD029134

Massoli P, Lambe AT, Ahern AT, Williams LR, Ehn M, Mikkilä J, et al. (2010). Relationship between aerosol oxidation level and hygroscopic properties of laboratory generated secondary organic aerosol (SOA) particles. Geophysical Research Letters, 37, L24801 10.1029/2010GL045258

Mauldin RL, Tanner DJ, Heath JA, Huebert BJ, & Eisele FL (1999). Observations of H2SO4 and MSA during PEM-Tropics-A. Journal of Geophysical Research, 104(D5), 5801–5816. 10.1029/98JD02612

McFiggans G, Artaxo P, Baltensperger U, Coe H, Facchini MC, Feingold G, et al. (2006). The effect of physical and chemical aerosol properties on warm cloud droplet activation. Atmospheric Chemistry and Physics, 6(9), 2593–2649. 10.5194/acp-6-2593-2006

Medina J, Nenes A, Sotiropoulou R-EP, Cottrell LD, Ziemba LD, Beckman PJ, & Griffin RJ (2007). Cloud condensation nuclei closure during the International Consortium for Atmospheric Research on Transport and Transformation 2004 campaign: Effects of size-resolved composition. Journal of Geophysical Research, 112, D10S31 10.1029/2006JD007588

Mei F, Setyan A, Zhang Q, & Wang J (2013). CCN activity of organic aerosols observed downwind of urban emissions during CARES. Atmospheric Chemistry and Physics, 13(24), 12,155–12,169. 10.5194/acp-13-12155-2013

Middlebrook AM, Bahreini R, Jimenez JL, & Canagaratna MR (2012). Evaluation of composition-dependent collection efficiencies for the aerodyne aerosol mass spectrometer using field data. Aerosol Science and Technology, 46(3), 258–271. 10.1080/02786826.2011.620041

Modini RL, Frossard AA, Ahlm L, Russell LM, Corrigan CE, Roberts GC, et al. (2015). Primary marine aerosol-cloud interactions off the coast of California. Journal of Geophysical Research: Atmospheres, 120, 4282–4303. 10.1002/2014JD022963

Moore RH, Bahreini R, Brock CA, Froyd KD, Cozic J, Holloway JS, et al. (2011). Hygroscopicity and composition of Alaskan Arctic CCN during April 2008. Atmospheric Chemistry and Physics, 11(22), 11,807–11,825. 10.5194/acp-11-11807-2011

Moore RH, Cerully K, Bahreini R, Brock CA, Middlebrook AM, & Nenes A (2012). Hygroscopicity and composition of California CCN during summer 2010. Journal of Geophysical Research, 117, D00V12 10.1029/2011JD017352

Murphy SM, Agrawal H, Sorooshian A, Padró LT, Gates H, Hersey S, et al. (2009). Comprehensive simultaneous shipboard and airborne characterization of exhaust from a modern container ship at sea. Environmental Science & Technology, 43(13), 4626–4640. 10.1021/es802413j [PubMed: 19673244]

Nenes A, Pandis SN, & Pilinis C (1998). ISORROPIA: A new thermodynamic equilibrium model for multiphase multicomponent inorganic aerosols. Aquatic Geochemistry, 4(1), 123–152. 10.1023/A:1009604003981

Oreopoulos L, & Platnick S (2008). Radiative susceptibility of cloudy atmospheres to droplet number perturbations: 2. Global analysis from MODIS. Journal of Geophysical Research, 113, D14S21 10.1029/2007JD009655

Paatero P, & Tapper U (1994). Positive matrix factorization: A non-negative factor model with optimal utilization of error estimates of data values. Environmetrics, 5(2), 111–126. 10.1002/env.3170050203

Petters MD, & Kreidenweis SM (2007). A single parameter representation of hygroscopic growth and cloud condensation nucleus activity. Atmospheric Chemistry and Physics, 7(8), 1961–1971. 10.5194/acp-7-1961-2007

Platnick S, & Twomey S (1994). Determining the susceptibility of cloud albedo to changes in droplet concentration with the advanced very high resolution radiometer. Journal of Applied Meteorology, 33(3), 334–347. 10.1175/1520-0450(1994)033<0334:DTSOCA>2.0.CO;2

Prabhakar G, Ervens B, Wang Z, Maudlin LC, Coggon MM, Jonsson HH, et al. (2014). Sources of nitrate in stratocumulus cloud water: Airborne measurements during the 2011 E-PEACE and 2013 NiCE studies. Atmospheric Environment, 97, 166–173. 10.1016/j.atmosenv.2014.08.019

Pringle KJ, Tost H, Pozzer A, Pöschl U, & Lelieveld J (2010). Global distribution of the effective aerosol hygroscopicity parameter for CCN activation. Atmospheric Chemistry and Physics, 10(12), 5241–5255. 10.5194/acp-10-5241-2010

Pruppacher HR, & Klett JD (1997). Microphysics of clouds and precipitation. Dordrecht, The Netherlands: Kluwer.

Quinn PK, Bates TS, Coffman DJ, & Covert DS (2008). Influence of particle size and chemistry on the cloud nucleating properties of aerosols. Atmospheric Chemistry and Physics, 8(4), 1029–1042. 10.5194/acp-8-1029-2008

Raes F (1995). Entrainment of free tropospheric aerosols as a regulating mechanism for cloud condensation nuclei in the remote marine boundary layer. Journal of Geophysical Research, 100(D2), 2893–2903. 10.1029/94JD02832

Randall DA, Coakley JA, Fairall CW, Kropfli RA, & Lenschow DH (1984). Outlook for research on subtropical marine stratiform clouds. Bulletin of the American Meteorological Society, 65(12), 1290–1301. 10.1175/1520-0477(1984)065<1290:OFROSM>2.0.CO;2

Ren J, Zhang F, Wang Y, Collins D, Fan X, Jin X, et al. (2018). Using different assumptions of aerosol mixing state and chemical composition to predict CCN concentrations based on field measurements in urban Beijing. Atmospheric Chemistry and Physics, 18(9), 6907–6921. 10.5194/acp-18-6907-2018

Reutter P, Su H, Trentmann J, Simmel M, Rose D, Gunthe SS, et al. (2009). Aerosol- and updraft-limited regimes of cloud droplet formation: Influence of particle number, size and hygroscopicity on the activation of cloud condensation nuclei (CCN). Atmospheric Chemistry and Physics, 9(18), 7067–7080. 10.5194/acp-9-7067-2009

Roberts G, Mauger G, Hadley O, & Ramanathan V (2006). North American and Asian aerosols over the eastern Pacific Ocean and their role in regulating cloud condensation nuclei. Journal of Geophysical Research, 111, D13205 10.1029/2005JD006661

Roberts GC, Day DA, Russell LM, Dunlea EJ, Jimenez JL, Tomlinson JM, et al. (2010). Characterization of particle cloud droplet activity and composition in the free troposphere and the boundary layer during INTEX-B. Atmospheric Chemistry and Physics, 10 (14), 6627–6644. 10.5194/acp-10-6627-2010

Roberts GC, & Nenes A (2005). A continuous-flow streamwise thermal-gradient CCN chamber for atmospheric measurements. Aerosol Science and Technology, 39(3), 206–221. 10.1080/027868290913988

Rose D, Gunthe SS, Mikhailov E, Frank GP, Dusek U, Andreae MO, & Pöschl U (2008). Calibration and measurement uncertainties of a continuous-flow cloud condensation nuclei counter (DMT-CCNC): CCN activation of ammonium sulfate and sodium chloride aerosol particles in theory and experiment. Atmospheric Chemistry and Physics, 8(5), 1153–1179. 10.5194/acp-8-1153-2008

Rose D, Gunthe SS, Su H, Garland RM, Yang H, Berghof M, et al. (2011). Cloud condensation nuclei in polluted air and biomass burning smoke near the mega-city Guangzhou, China—Part 2: Size-resolved aerosol chemical composition, diurnal cycles, and externally mixed weakly CCN-active soot particles. Atmospheric Chemistry and Physics, 11(6), 2817–2836. 10.5194/acp-11-2817-2011

Rose D, Nowak A, Achtert P, Wiedensohler A, Hu M, Shao M, et al. (2010). Cloud condensation nuclei in polluted air and biomass burning smoke near the mega-city Guangzhou, China—Part 1: Size-resolved measurements and implications for the modeling of aerosol particle hygroscopicity and CCN activity. Atmospheric Chemistry and Physics, 10(7), 3365–3383. 10.5194/acp-10-3365-2010

Rosenfeld D (2006). Aerosol-cloud interactions control of earth radiation and latent heat release budgets. Space Science Reviews, 125(1–4), 149–157. 10.1007/s11214-006-9053-6

Rosenfeld D, Andreae MO, Asmi A, Chin M, de Leeuw G, Donovan DP, et al. (2014). Global observations of aerosol-cloud-precipitation-climate interactions. Reviews of Geophysics, 52, 750–808. 10.1002/2013RG000441

Rosenfeld D, Zhu Y, Wang M, Zheng Y, Goren T, & Yu S (2019). Aerosol-driven droplet concentrations dominate coverage and water of oceanic low-level clouds. Science, 363, eaav0566 10.1126/science.aav0566 [PubMed: 30655446]

Rothenberg D, Avramov A, & Wang C (2018). On the representation of aerosol activation and its influence on model-derived estimates of the aerosol indirect effect. Atmospheric Chemistry and Physics, 18(11), 7961–7983. 10.5194/acp-18-7961-2018

Royalty TM, Phillips BN, Dawson KW, Reed R, Meskhidze N, & Petters MD (2017). Aerosol properties observed in the subtropical North Pacific boundary layer. Journal of Geophysical Research: Atmospheres, 122, 9990–10,012. 10.1002/2017JD026897

Russell LM, Sorooshian A, Seinfeld JH, Albrecht BA, Nenes A, Ahlm L, et al. (2013). Eastern Pacific emitted aerosol cloud experiment. Bulletin of the American Meteorological Society, 94(5), 709–729. 10.1175/BAMS-D-12-00015.1

Sanchez KJ, Russell LM, Modini RL, Frossard AA, Ahlm L, Corrigan CE, et al. (2016). Meteorological and aerosol effects on marine cloud microphysical properties. Journal of Geophysical Research: Atmospheres, 121, 4142–4161. 10.1002/2015JD024595

Sánchez-Gácita M, Longo KM, Freire JLM, Freitas SR, & Martin ST (2017). Impact of mixing state and hygroscopicity on CCN activity of biomass burning aerosol in Amazonia. Atmospheric Chemistry and Physics, 17(3), 2373–2392. 10.5194/acp-17-2373-2017

Seinfeld JH, Bretherton C, Carslaw KS, Coe H, DeMott PJ, Dunlea EJ, et al. (2016). Improving our fundamental understanding of the role of aerosol–cloud interactions in the climate system. PNAS, 113(21), 5781–5790. 10.1073/pnas.1514043113 [PubMed: 27222566]

Sorooshian A, Anderson B, Bauer SE, Braun RA, Cairns B, Crosbie E, et al. (2019). Aerosol-cloud-meteorology interaction airborne field investigations: Using lessons learned from the US West Coast in the design of ACTIVATE off the US East Coast. Bulletin of the American Meteorological Society, 100(8), 1511–1528. 10.1175/BAMS-D-18-0100.1

Sorooshian A, Lu M-L, Brechtel FJ, Jonsson H, Feingold G, Flagan RC, & Seinfeld JH (2007). On the source of organic acid aerosol layers above clouds. Environmental Science & Technology, 41(13), 4647–4654. 10.1021/es0630442 [PubMed: 17695910]

Sorooshian A, MacDonald AB, Dadashazar H, Bates KH, Coggon MM, Craven JS, et al. (2017). A multi-year data set on aerosol-cloud-precipitation-meteorology interactions for marine stratocumulus clouds. Figshare Dataset. 10.6084/m9.figshare.5099983.v10

Sorooshian A, MacDonald AB, Dadashazar H, Bates KH, Coggon MM, Craven JS, et al. (2018). A multi-year data set on aerosol-cloud-precipitation-meteorology interactions for marine stratocumulus clouds. Scientific Data, 5, 180026 10.1038/sdata.2018.26 [PubMed: 29485627]

Sorooshian A, Ng NL, Chan AWH, Feingold G, Flagan RC, & Seinfeld JH (2007). Particulate organic acids and overall water-soluble aerosol composition measurements from the 2006 Gulf of Mexico Atmospheric Composition and Climate Study (GoMACCS). Journal of Geophysical Research, 112, D13201 10.1029/2007JD008537

Sorooshian A, Padró LT, Nenes A, Feingold G, McComiskey A, Hersey SP, et al. (2009). On the link between ocean biota emissions, aerosol, and maritime clouds: Airborne, ground, and satellite measurements off the coast of California. Global Biogeochemical Cycles, 23, GB4007 10.1029/2009GB003464

Sotiropoulou R-EP, Nenes A, Adams PJ, & Seinfeld JH (2007). Cloud condensation nuclei prediction error from application of Köhler theory: Importance for the aerosol indirect effect. Journal of Geophysical Research, 112, D12202 10.1029/2006JD007834

Stein AF, Draxler RR, Rolph GD, Stunder BJB, Cohen MD, & Ngan F (2015). NOAA's HYSPLIT atmospheric transport and dispersion modeling system. Bulletin of the American Meteorological Society, 96(12), 2059–2077. 10.1175/BAMS-D-14-00110.1

Stevens B, & Brenguier J-L (2009). Cloud-controlling factors: Low clouds. Cambridge, MA: The MIT Press

Thalman R, de Sá SS, Palm BB, Barbosa HMJ, Pöhlker ML, Alexander ML, et al. (2017). CCN activity and organic hygroscopicity of aerosols downwind of an urban region in central Amazonia: Seasonal and diel variations and impact of anthropogenic emissions. Atmospheric Chemistry and Physics, 17(19), 11,779–11,801. 10.5194/acp-17-11779-2017

Twomey S (1977). The influence of pollution on the shortwave albedo of clouds. Journal of the Atmospheric Sciences, 34(7), 1149–1152. 10.1175/1520-0469(1977)034<1149:TIOPOT>2.0.CO;2

Ueda S, Miura K, Kawata R, Furutani H, Uematsu M, Omori Y, & Tanimoto H (2016). Number–size distribution of aerosol particles and new particle formation events in tropical and subtropical Pacific Oceans. Atmospheric Environment, 142, 324–339. 10.1016/j.atmosenv.2016.07.055

VanReken TM, Rissman TA, Roberts GC, Varutbangkul V, Jonsson HH, Flagan RC, & Seinfeld JH (2003). Toward aerosol/cloud condensation nuclei (CCN) closure during CRYSTAL-FACE. Journal of Geophysical Research, 108(D20), 4633 10.1029/2003JD003582

Wang J, Cubison MJ, Aiken AC, Jimenez JL, & Collins DR (2010). The importance of aerosol mixing state and size-resolved composition on CCN concentration and the variation of the importance with atmospheric aging of aerosols. Atmospheric Chemistry and Physics, 10(15), 7267–7283. 10.5194/acp-10-7267-2010

Wang J, Lee Y-N, Daum PH, Jayne J, & Alexander ML (2008). Effects of aerosol organics on cloud condensation nucleus (CCN) concentration and first indirect aerosol effect. Atmospheric Chemistry and Physics, 8(21), 6325–6339. 10.5194/acp-8-6325-2008

Wang J, Shilling JE, Liu J, Zelenyuk A, Bell DM, Petters MD, et al. (2019). Cloud droplet activation of secondary organic aerosol is mainly controlled by molecular weight, not water solubility. Atmospheric Chemistry and Physics, 19(2), 941–954. 10.5194/acp-19-941-2019

Wang Z, Ramirez MM, Dadashazar H, MacDonald AB, Crosbie E, Bates KH, et al. (2016). Contrasting cloud composition between coupled and decoupled marine boundary layer clouds. Journal of Geophysical Research: Atmospheres, 121, 11,679–11,691. 10.1002/2016JD025695

Ward DS, Eidhammer T, Cotton WR, & Kreidenweis SM (2010). The role of the particle size distribution in assessing aerosol composition effects on simulated droplet activation. Atmospheric Chemistry and Physics, 10(12), 5435–5447. 10.5194/acp-10-5435-2010

Wonaschütz A, Coggon M, Sorooshian A, Modini R, Frossard AA, Ahlm L, et al. (2013). Hygroscopic properties of smoke-generated organic aerosol particles emitted in the marine atmosphere. Atmospheric Chemistry and Physics, 13(19), 9819–9835. 10.5194/acp-13-9819-2013

Wood R (2012). Stratocumulus clouds. Monthly Weather Review, 140(8), 2373–2423. 10.1175/MWR-D-11-00121.1

Yakobi-Hancock JD, Ladino LA, Bertram AK, Huffman JA, Jones K, Leaitch WR, et al. (2014). CCN activity of size-selected aerosol at a Pacific coastal location. Atmospheric Chemistry and Physics, 14(22), 12,307–12,317. 10.5194/acp-14-12307-2014

Zhao DF, Buchholz A, Kortner B, Schlag P, Rubach F, Kiendler-Scharr A, et al. (2015). Size-dependent hygroscopicity parameter (κ) and chemical composition of secondary organic cloud condensation nuclei. Geophysical Research Letters, 42, 10,920–10,928. 10.1002/2015GL066497

Zheng Y, Rosenfeld D, & Li Z (2016). Quantifying cloud base updraft speeds of marine stratocumulus from cloud top radiative cooling. Geophysical Research Letters, 43, 11,407–11,413. 10.1002/2016GL071185

Key Points:

- Aerosol hygroscopicity exhibited substantial temporal variability in the MBL
- Errors in predicted MBL CCN concentrations produced by assuming a constant aerosol size distribution or hygroscopicity are discussed
- Sensitivity of simulated CDNC to hygroscopicity is maximized in marine clouds with either very weak or relatively strong updraft velocities

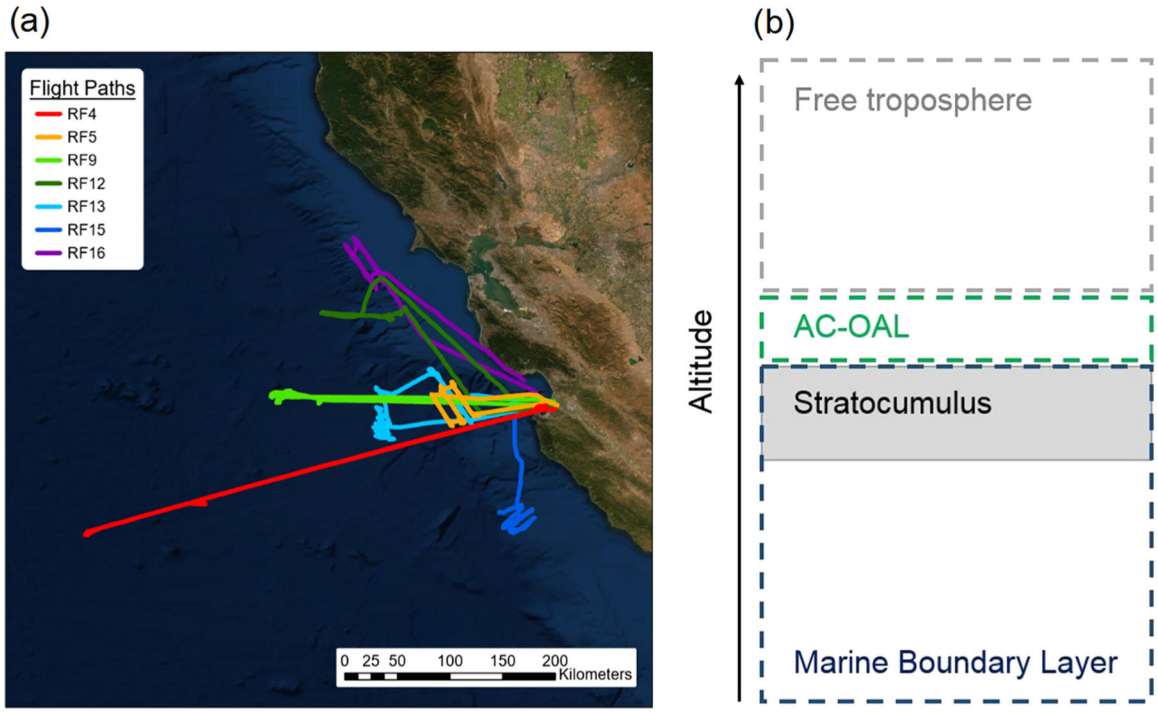

Figure 1.

(a) Trajectories of the seven MACAWS research flights analyzed in this study. (b) Relative vertical locations of the marine boundary layer, the above-cloud organic-aerosol layer (AC-OAL), and the free troposphere.

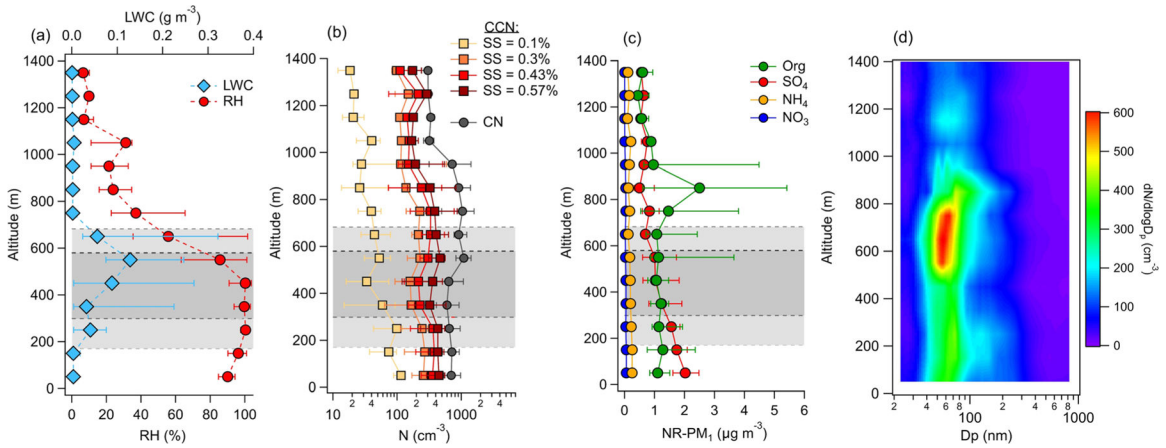

Figure 2.

Vertical profiles of (a) RH and LWC, (b) CCN and CN concentrations, and (c) non-refractory (NR) PM_1 component mass loadings for the seven RFs in Figure 1. Markers represent median values, while horizontal bars span the interquartile range. (d) Vertical contour plot of median size distributions measured during the seven RFs. The dark grey region in panels a–c represents the average stratocumulus cloud depth (avg. cloud top height ≈ 570 m; avg. cloud bottom height ≈ 300 m). The lighter grey region represents the standard deviation of cloud top and bottom heights (e.g., avg. cloud top + cloud top height S.D. ≈ 680 m).

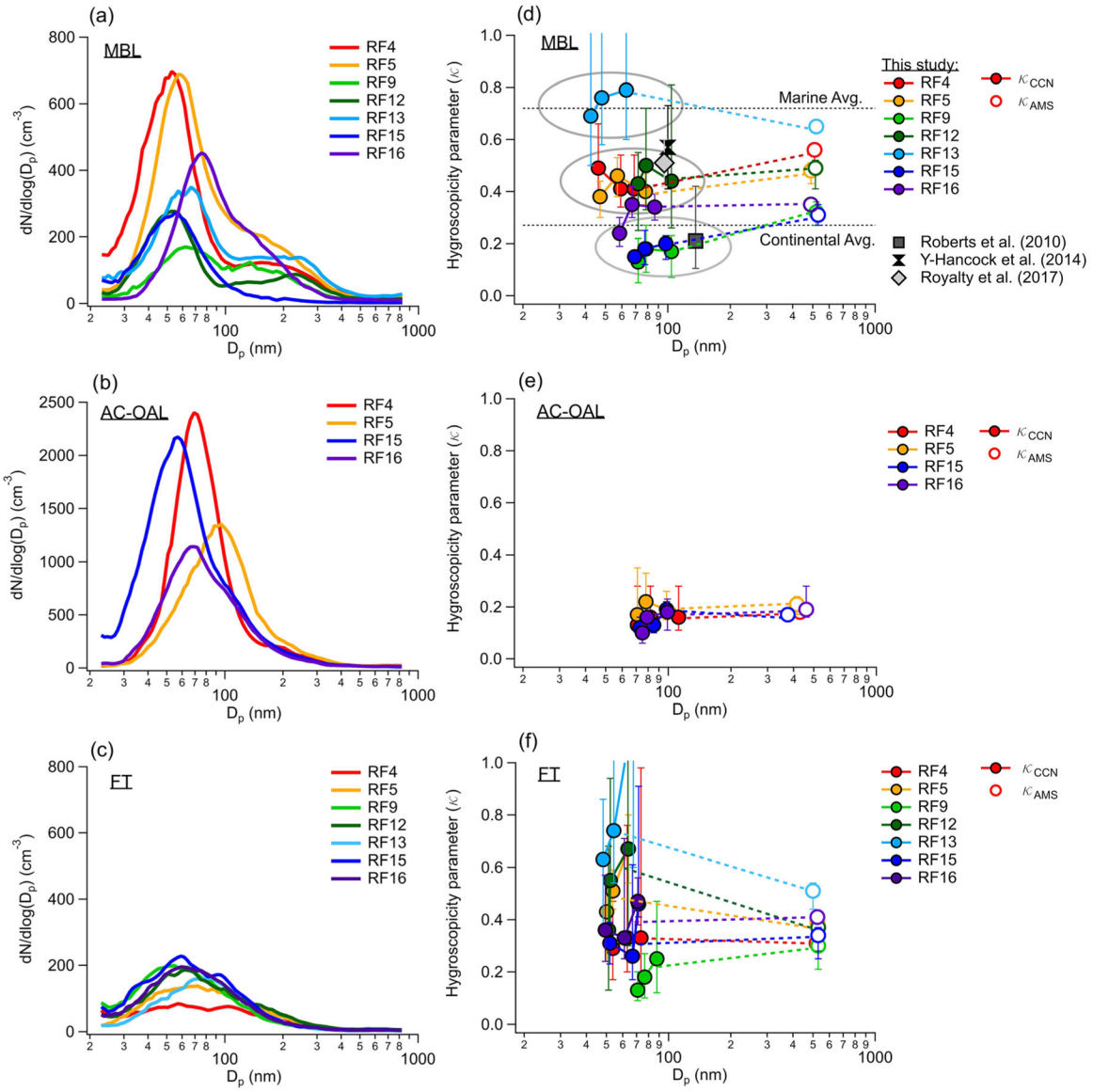

Figure 3.

Median aerosol size distributions (a–c) and hygroscopicities (κ_{CCN} and κ_{AMS}) (d–f) measured in the marine boundary layer (MBL), above-cloud organic aerosol layer (AC-OAL), and free troposphere (FT), during the seven RFs. κ_{AMS} values are calculated assuming κ_{org} = 0.1 and are plotted at the median of the cumulative aerosol volume distribution. Vertical bars represent the interquartile range of hygroscopicity measurements. Previously observed values in the MBL are included for reference in (d), as are typical values for continental and marine environments from Pringle et al. (2010).

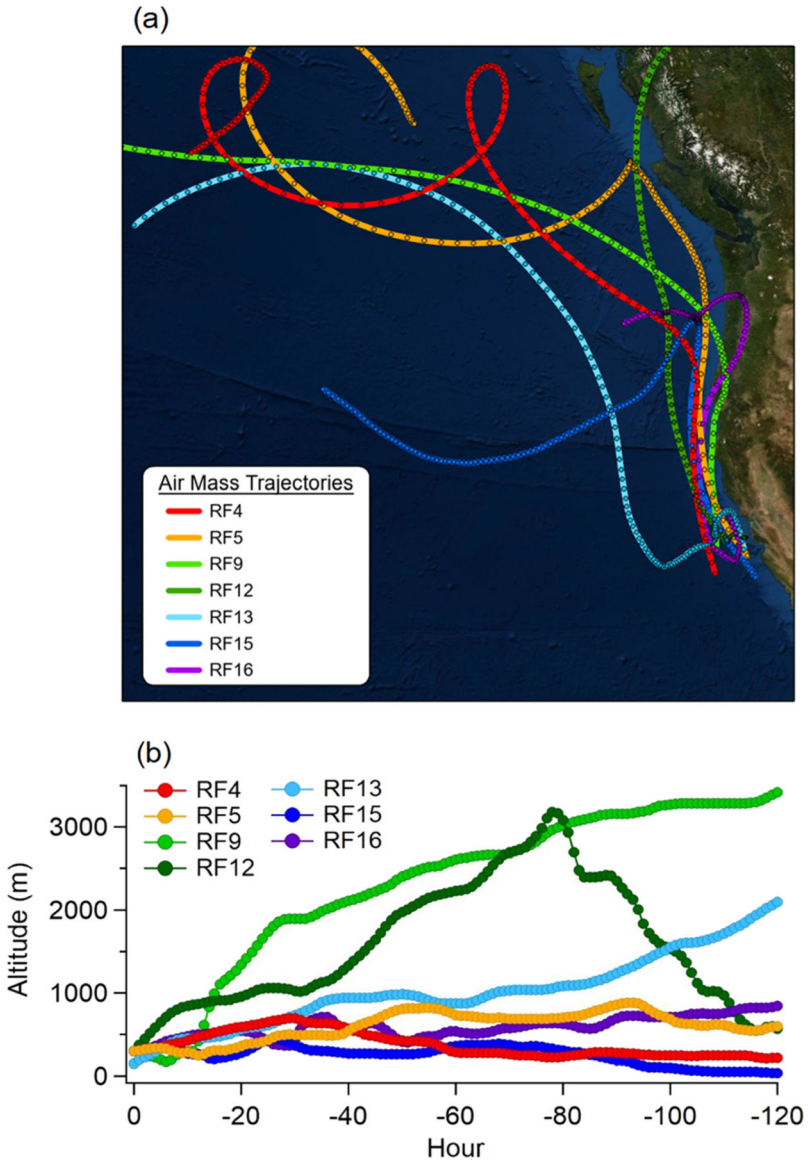

Figure 4.

(a) 120-hr air mass backward trajectories calculated using the HYSPLIT model (Stein et al., 2015) from the approximate midpoint of each flight path at an altitude representative of the marine boundary layer. For six of the seven flights, the starting altitude was 300 m, while the starting altitude for the RF13 trajectory was 150 m due to the shallow height of the boundary layer. (b) Air mass altitude during the 120-hr transit to the measurement site.

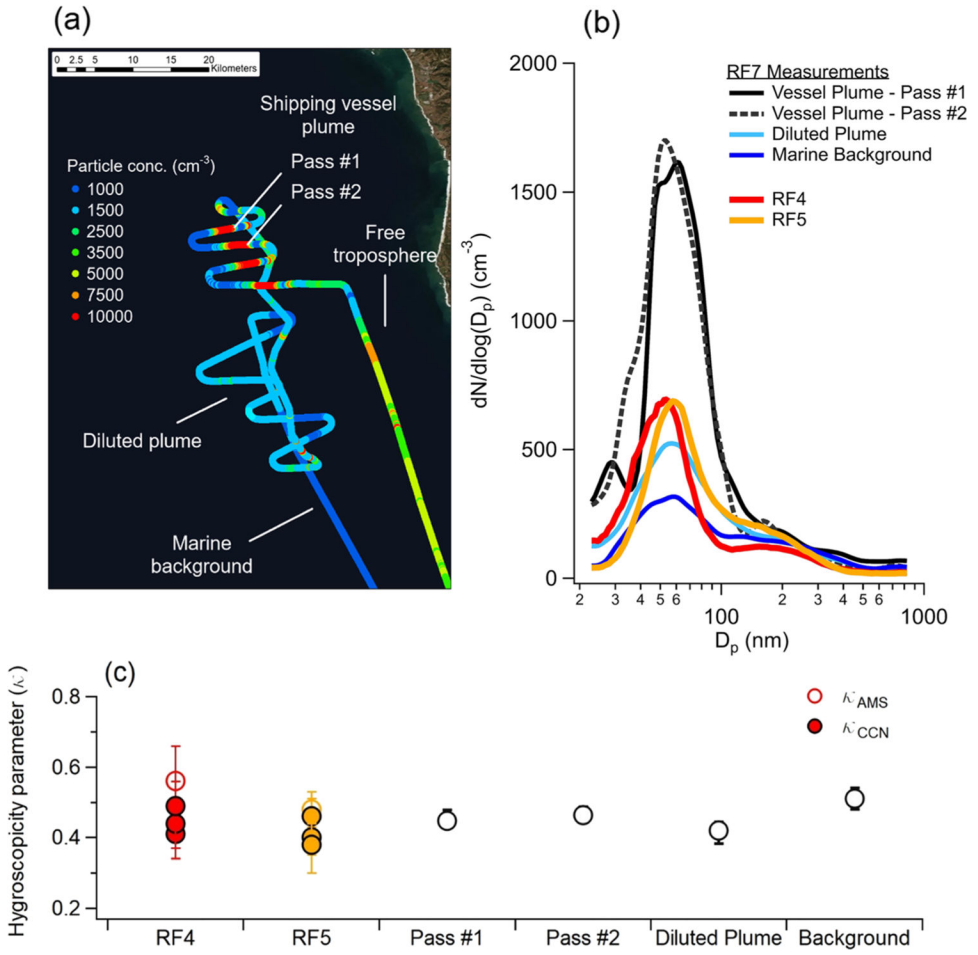

Figure 5.

(a) Map of the Twin Otter trajectory during repeated sampling of the exhaust plume from a 330-m shipping vessel during RF7. Points are colored by the particle concentration measured by the CPC, and individual segments of the flight path are labeled. (b) Aerosol size distributions measured during the labeled segments in (a) compared to median distributions measured during RF4 and RF5. (c) Comparison of κ values derived from CCN and AMS measurements in RF4 and RF5 with those derived from AMS measurements during the flight segments shown in (a).

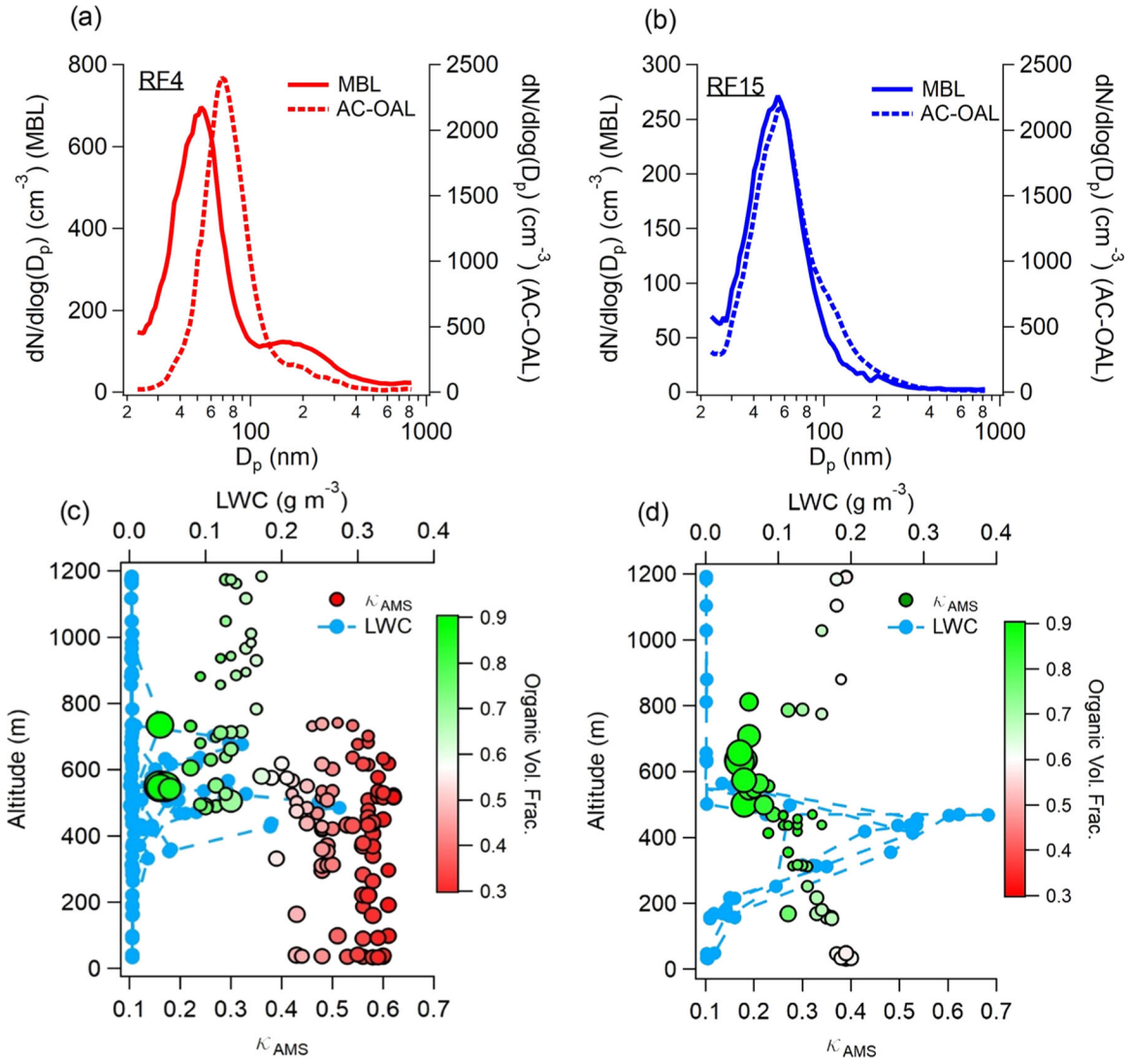

Figure 6.

(Top) Median aerosol size distributions measured in the marine boundary layer (MBL) and above-cloud organic aerosol layer (AC-OAL) during RF4 (a) and RF15 (b). (Bottom) Vertical profile of AMS-derived hygroscopicity (κ_{AMS}) and liquid water content (LWC) during each flight. Values of κ_{AMS} are colored by the organic volume fraction measured by the AMS to aid interpretation of the figure.

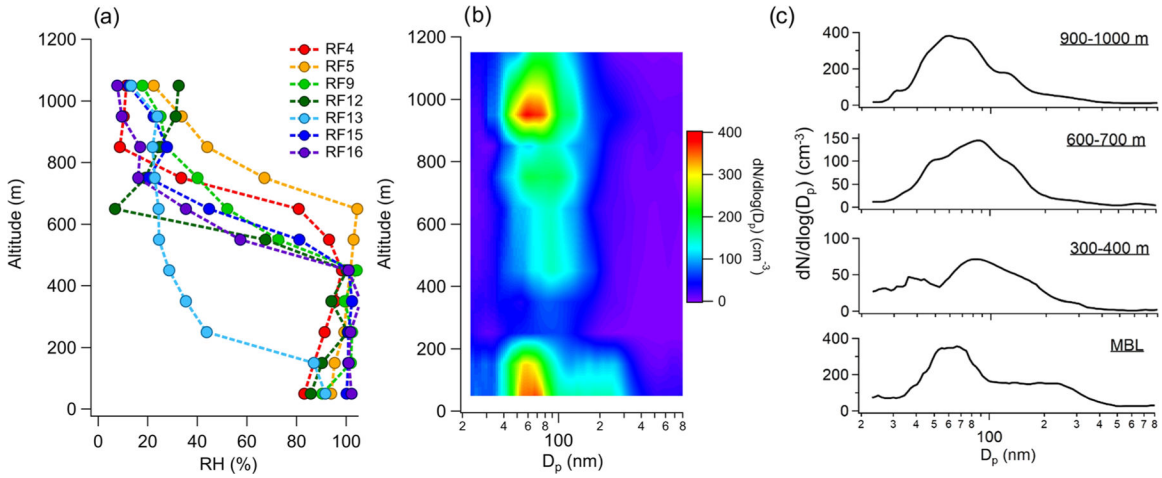

Figure 7.

(a) Measured relative humidity vertical profile during each flight, demonstrating the reduced marine boundary layer (MBL) height during RF13. (b) Vertical profile of aerosol number size distributions during RF13. (c) Individual aerosol size distributions at different altitudes during RF13.

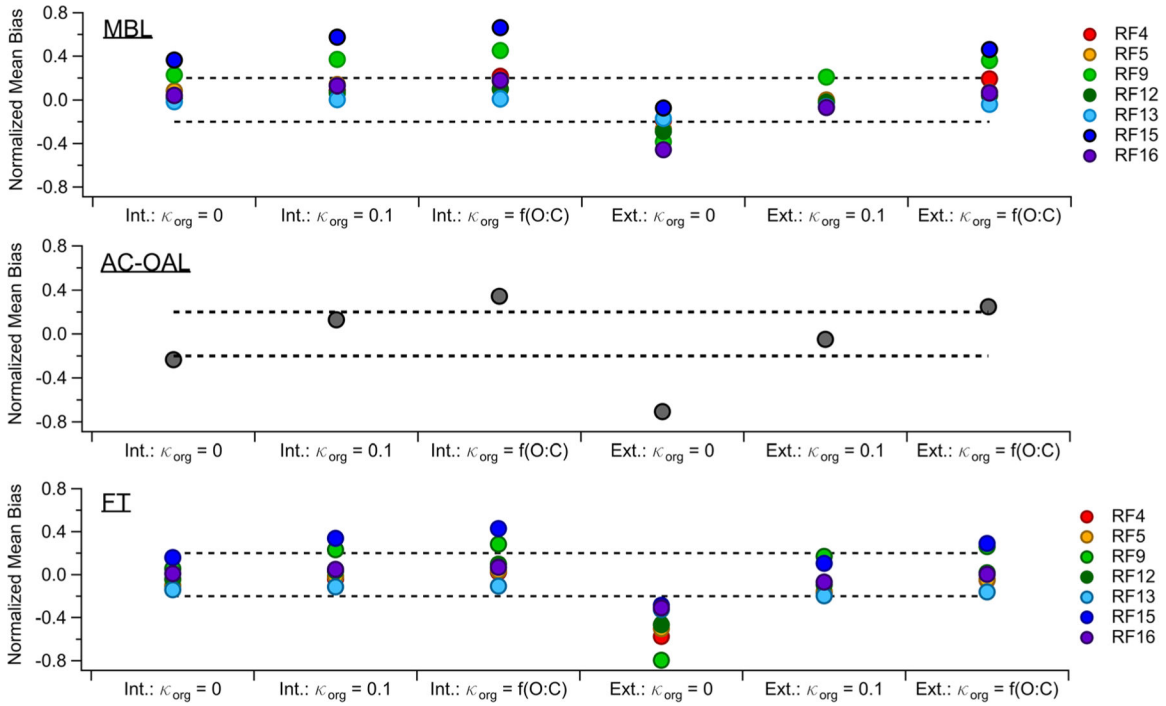

Figure 8.

Normalized mean bias resulting from CCN closure analysis performed on data from each flight. A value of 0.2 is equivalent to an average overprediction of 20%. Int. indicates aerosol were assumed internally mixed, while Ext. indicates organic and inorganic aerosol were assumed to be externally mixed. κ_{org} represents the assumed hygroscopicity of the organic aerosol component, and f(O:C) indicates κ_{org} was calculated based on the bulk aerosol O:C ratio using the parameterization derived by Lambe et al. (2011).

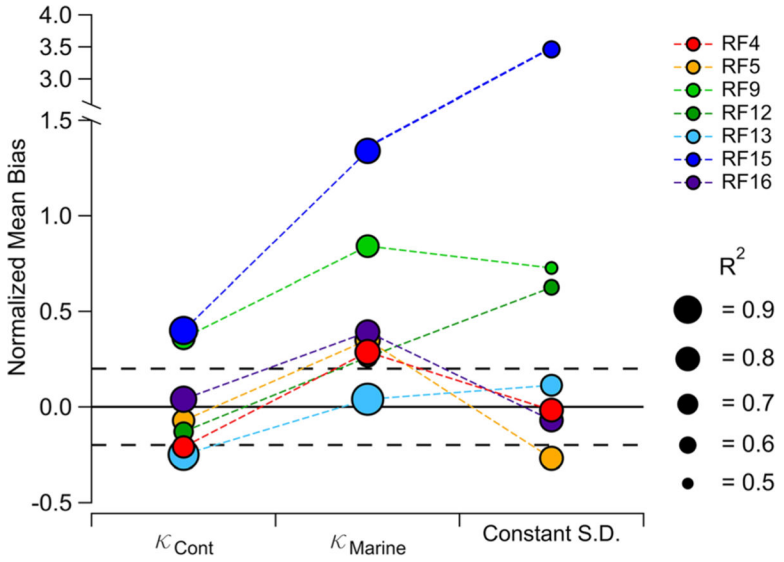

Figure 9.

Normalized mean bias resulting from additional CCN closure analyses performed on data from each flight. κ_{Cont} and κ_{Marine} refer to analyses assuming a constant κ equivalent to values representative of continental (0.27) and marine (0.72) environments (Pringle et al., 2010). The Constant S.D. case assumes a constant aerosol number size distribution equivalent to the median value observed in the MBL during the campaign. Blacked dashed lines indicate closure error of ±20%. Marker size corresponds to the R^2 value computed from a linear fit of observed and predicted CCN from each flight. Note the split in the *y*-axis.

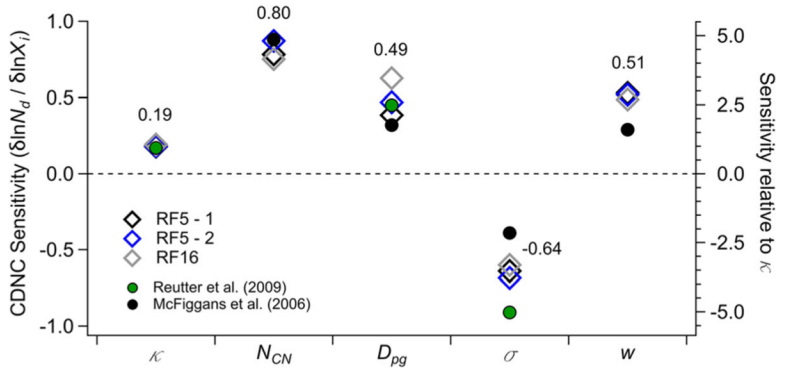

Figure 10.

Sensitivity of calculated CDNC to accumulation mode aerosol hygroscopicity (κ), below-cloud aerosol particle number concentration (N_{CN}), accumulation mode geometric mean diameter (D_{pg}), accumulation mode standard deviation (σ), and updraft velocity (w). Data obtained during three cloud sampling passes were used as model constraints and are listed in Table 5. Numbers near each group of symbols represent average values from simulations in this study. Green symbols correspond to values reported by Reutter et al. (2009) for the transitional activation regime, while those in black correspond to values reported by McFiggans et al. (2006).

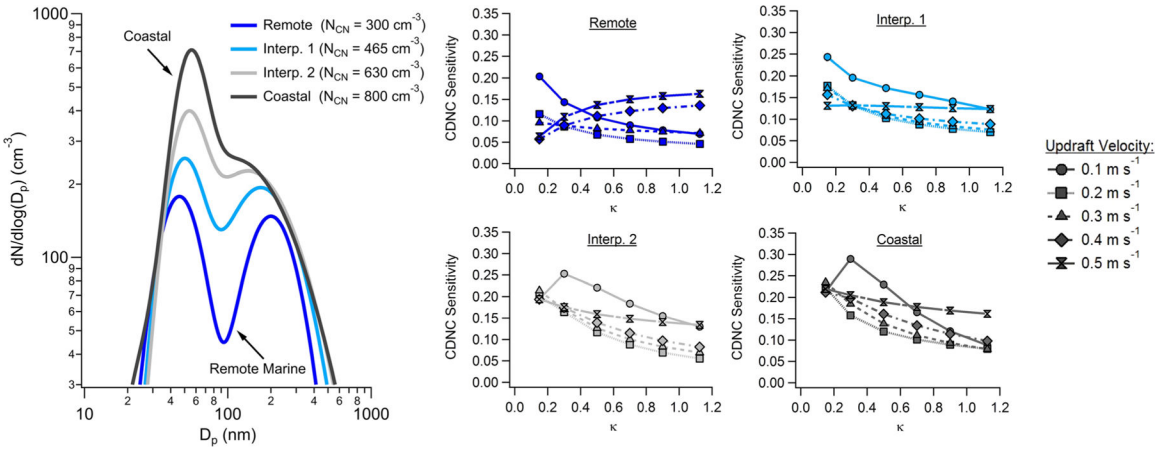

Figure 11.

(Left) Aerosol number size distributions used as aerosol-cloud-parcel model inputs and (right) local CDNC sensitivities to aerosol hygroscopicity calculated using five updraft velocities. N_{CN} refers to the aerosol number concentration represented by each aerosol size distribution.

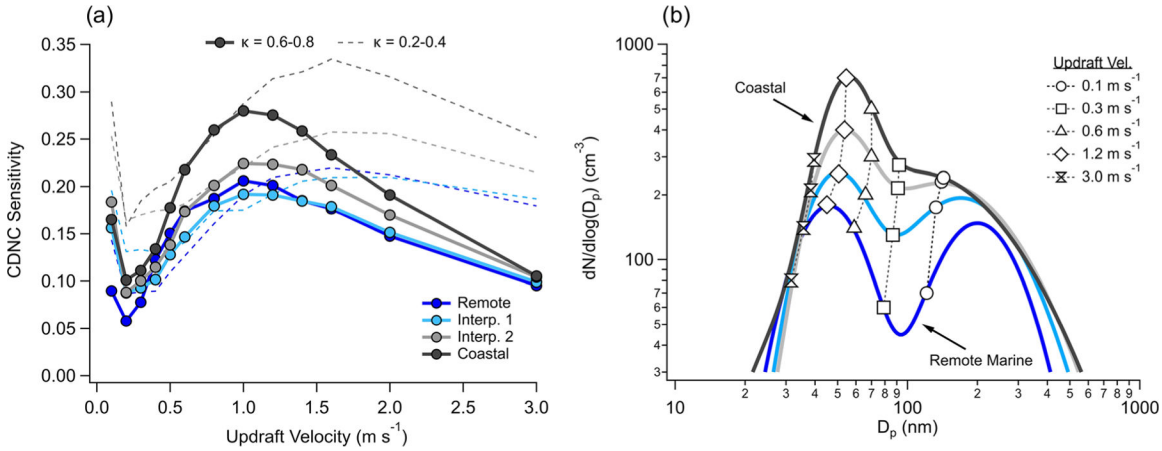

Figure 12.

(a) Simulated local CDNC sensitivity to aerosol hygroscopicity in the range $\kappa = 0.6–0.8$ and $\kappa = 0.2–0.4$ as a function of updraft velocity. (b) Critical diameters (markers) calculated at the maximum supersaturation predicted by the aerosol-cloud-parcel model for five different updraft velocities assuming $\kappa = 0.6$.

Table 1

Median Aerosol Number (N) and Cloud Condensation Nuclei (CCN) Concentrations Measured in the Marine Boundary Layer (MBL), Above-Cloud Organic Aerosol Layer (AC-OAL), and Free Troposphere (FT)

Location	N (cm^{-3})	CCN: 0.1% (cm^{-3})	CCN: 0.3% (cm^{-3})	CCN: 0.43% (cm^{-3})	CCN: 0.57% (cm^{-3})
MBL	754 (509–978)	75 (33–106)	194 (146–285)	302 (187–410)	410 (229–522)
AC-OAL	1,662 (1,303–1,959)	58 (41–84)	363 (260–537)	574 (403–876)	781 (539–1,051)
FT	333 (296–555)	21 (14–35)	115 (89–145)	144 (102–194)	162 (118–240)

Note. Values in parentheses represent the interquartile range. CCN concentrations are provided as a function of the instrument supersaturation (%).

Table 2

Median Mass Loadings of Total Non-Refractory PM1 ($NR\text{-}PM_1$), and Organic (Org.), Sulfate (SO_4), Ammonium (NH_4), and Nitrate (NO_3) Aerosol Components in the Marine Boundary Layer (MBL), Above-Cloud Organic Aerosol Layer (AC-OAL), and Free Troposphere (FT)

Location	$NR\text{-}PM_1$ ($\mu g\ m^{-3}$)	Org. ($\mu g\ m^{-3}$)	SO_4 ($\mu g\ m^{-3}$)	NH_4 ($\mu g\ m^{-3}$)	NO_3 ($\mu g\ m^{-3}$)
MBL	2.8 (2.3–2.5)	1.1 (0.8–1.4)	1.5 (0.9–2.0)	0.2 (0.2–0.3)	0.0 (0.0–0.1)
AC-OAL	5.5 (4.5–7.5)	4.4 (3.2–6.1)	0.7 (0.6–1.1)	0.2 (0.2–0.3)	0.1 (0.0–0.1)
FT	1.5 (1.2–2.1)	0.7 (0.5–1.0)	0.6 (0.4–0.7)	0.1 (0.1–0.2)	0.0 (0.0–0.0)

Note. Values in parentheses represent the interquartile range.

Table 3

Median Values of the AMS-Derived (κ_{AMS}) and CCN-Derived (κ_{CCN}) Hygroscopicity Factor Measured in the Marine Boundary Layer (MBL), Above-Cloud Organic Aerosol Layer (AC-OAL), and Free Troposphere (FT)

Location	κ_{AMS}	κ_{CCN}: 0.3%	κ_{CCN}: 0.43%	κ_{CCN}: 0.57%
MBL	0.45 (0.35–0.52)	0.39 (0.20–0.61)	0.35 (0.24–0.50)	0.40 (0.27–0.54)
AC-OAL	0.19 (0.17–0.25)	0.13 (0.08–0.20)	0.19 (0.14–0.25)	0.17 (0.12–0.27)
FT	0.37 (0.30–0.43)	0.32 (0.18–0.65)	0.50 (0.29–0.88)	0.37 (0.21–0.72)

Note. Values in parentheses represent the interquartile range. κ_{CCN} are provided as a function of the instrument supersaturation (%).

Table 4

Calculated Aitken Mode Organic (f_{org}) and Inorganic (f_{inorg}) Volume Fractions Based on Median κ_{CCN} Values Derived From CCN Measurements at SS = 0.43% for MBL Measurements During Each Flight

		Inorg. = $(NH_4)_2SO_4$		Inorg. = H_2SO_4	
Flight	**κ_{CCN} − SS = 0.43%**	f_{org}	f_{inorg}	f_{org}	f_{inorg}
RF4	0.41	0.39	0.61	0.61	0.39
RF5	0.46	0.29	0.71	0.55	0.45
RF9	0.18	0.84	0.16	0.90	0.10
RF12	0.50	0.22	0.78	0.50	0.50
RF13	0.76	~	~	0.18	0.82
RF15	0.18	0.84	0.16	0.90	0.10
RF16	0.28	0.65	0.35	0.78	0.22

Note. Values of f_{org} and f_{inorg} are calculated assuming the inorganic aerosol component is either ammonium sulfate ($(NH_4)_2SO_4$) or sulfuric acid (H_2SO_4). Note that the hygroscopicity measured during RF13 cannot be reproduced assuming the inorganic component is entirely $(NH_4)_2SO_4$.

Table 5

Below-Cloud Aerosol and Meteorological Data Used as Aerosol-Cloud-Parcel Model Constraints for Calculation of CDNC Sensitivities Depicted in Figure 10

Parameter	RF5–1	RF5–2	RF16
$N_{CN,\ \mathrm{Aitken}}$ (cm^{-3})	296	301	128
$D_{pg,\ \mathrm{Aitken}}$ (nm)	55	57	70
σ_{Aitken}	1.27	1.27	1.24
κ_{Aitken}	0.36	0.42	0.21
$N_{CN,\ \mathrm{Accum.}}$ (cm^{-3})	492	465	406
$D_{pg,\ \mathrm{Accum.}}$ (nm)	104	109	124
$\sigma_{\mathrm{Accum.}}$	2.21	2.20	1.96
$\kappa_{\mathrm{Accum.}}$	0.37	0.34	0.28
w ($m\ s^{-1}$)	0.22	0.26	0.25
w/N_{CN} ($m\ s^{-1}\ cm^{-3}$)	2.8×10^{-4}	3.4×10^{-4}	4.7×10^{-4}
Activation Regime	Trans.	Trans.	Trans.

Note. "Activation Regime" refers to the classifications of cloud droplet formation environments developed by Reutter et al. (2009). "Trans." = transitional.